
Detecting Anomalous Inputs to DNN Classifiers By Joint Statistical Testing at the Layers

Jayaram Raghuram Varun Chandrasekaran Somesh Jha
Suman Banerjee

University of Wisconsin - Madison

{jayaramr, chandrasekaran, jha, suman}@cs.wisc.edu

Abstract

Detecting anomalous inputs, such as adversarial and out-of-distribution (OOD) inputs, is critical for classifiers deployed in real-world applications, especially deep neural network (DNN) classifiers that are known to be brittle on such inputs. We propose an unsupervised statistical testing framework for detecting such anomalous inputs to a trained DNN classifier based on its internal layer representations. By calculating test statistics at the input and intermediate-layer representations of the DNN, conditioned individually on the predicted class and on the true class of labeled training data, the method characterizes their class-conditional distributions on natural inputs. Given a test input, its extent of non-conformity with respect to the training distribution is captured using p-values of the class-conditional test statistics across the layers, which are then combined using a scoring function designed to score high on anomalous inputs. We focus on adversarial inputs, which are an important class of anomalous inputs, and also demonstrate the effectiveness of our method on general OOD inputs. The proposed framework also provides an alternative class prediction that can be used to correct the DNN's prediction on (detected) adversarial inputs. Experiments on well-known image classification datasets with strong adversarial attacks, including a custom attack method that uses the internal layer representations of the DNN, demonstrate that our method outperforms or performs comparably with five state-of-the-art detection methods.

1 Introduction

Deep neural networks (DNNs) have achieved impressive performance on a variety of challenging machine learning (ML) problems such as image classification, object detection, speech recognition, and natural language processing [1–4]. However, it is well-known that DNN classifiers can be highly inaccurate on test inputs from outside the training distribution [5–8]. Such anomalous inputs can arise in real-world settings either unintentionally due to external factors, or due to malicious adversaries that intend to cause mis-classifications in the DNN and disrupt the system [9, 10]. In either case, it becomes critical to have a defense mechanism that can detect such anomalous inputs, and take suitable corrective action (*e.g.*, abstain from predicting [11, 12] or provide an alternate class prediction).

In this work, we propose ReBeL (Reading Between the Layers), a novel method for detecting anomalous inputs to a DNN classifier, focusing on the special cases of adversarial [6, 13–16] and OOD [7, 17, 18] samples. ReBeL utilizes the rich information at the intermediate layer representations (activations) of a DNN to obtain a better understanding of the patterns produced by anomalous inputs for detection. Our method is unsupervised, *i.e.*, it does not utilize a specific class of anomalous samples for learning or tuning its parameters. While a number of prior works have addressed the problem of adversarial and OOD detection [19–24], including ones that utilize intermediate layer

representations of a DNN [20–23, 25–29], some key limitations persist, that we propose to address in this work.

Limitations of prior work: Detection methods that extract specific properties or attributes from the layer representations and train supervised classifiers to discriminate anomalous inputs from natural inputs [19, 22, 23, 29] have to be presented with a broad sampling of anomalous inputs for training, which assumes prior knowledge of the anomalies (*e.g.*, adversarial attack type and parameters). Such methods often need to configure hyper-parameters based on the training data (using hold-out or cross-validation). As a result, they may be effective only against the particular (or similar) types of anomalies used for training. It has been shown that a majority of the current detection methods fail to handle unseen and adaptive adversaries that may be aware of the defense mechanism [30, 31]. On the other hand, unsupervised detection methods that are usually based on density (generative) modeling of the DNN layer representations [19, 26, 28] are not well suited to handle the (often very) high dimensional layer representations. Finally, we observe that detection methods often do not use the predicted class of the DNN [23, 29] to focus on class-conditional properties of the layer representations, which we have found leads to improved detection performance.

Our contributions can be summarized as follows:

- We propose a novel framework for unsupervised detection of anomalous inputs to a DNN classifier that effectively combines class-conditional test statistics extracted from the DNN’s layer representations into a statistically-grounded scoring method. The proposed framework is modular in its choice of test statistics at the DNN layers, which allows scoring methods from a number of existing works to be used as test statistics (*e.g.*, [23, 32, 33])¹.
- We show that ReBeL can defend a DNN classifier by simultaneously detecting and providing an alternate class prediction for inputs detected as adversarial.
- The importance of designing an adaptive defense-aware adversary has been underscored in the literature [30, 31]. We propose and evaluate against an adversarial attack that focuses on defenses (such as ours) that use the k -nearest neighbors of the layer representations of the DNN.

The rest of the paper is organized as follows. In § 2, we provide a background on adversarial and OOD detection and discuss related works. In § 3, we describe the proposed method, including 1) test statistics and p-values calculated from the DNN layers (§ 3.2 and § 3.3), 2) scoring methods for combining the test statistics for adversarial and OOD detection (§ 3.4 and § 3.5), 3) a method for correcting the class prediction of the DNN on adversarial inputs (§ 3.6), and 4) a multinomial test statistic derived from the class counts of the k -nearest neighbors of a layer representation (§ 3.7). In § 4, we propose a custom attack method for generating adversarial samples that is based on the input and internal layer representations. Implementation details and experimental results are given in § 5, followed by conclusions in § 6.

2 Background and Related Work

2.1 Adversarial Attacks

Adversarial attacks may be broadly classified into training-time or data poisoning attacks and test-time or evasion attacks [10]. Data poisoning attacks focus on tampering with the training set of a learning algorithm by introducing malicious input patterns that steer the learning algorithm to a sub-optimal solution, causing degradation in performance [34–36]. Evasion attacks focus on tampering with test inputs to an already-trained ML model such that the model predicts incorrectly on them. In both cases, an adversary aims to modify the inputs in such a way that the changes are not easily perceived by a human or flagged by a detector. For example, a test image of the digit 1 may be modified by introducing minimal perturbations to the pixels such that a classifier is fooled into classifying it as the digit 7, while the image still looks like the digit 1 to a human. Our focus in this work is on test-time evasion attacks.

Given a test input \mathbf{x} from class c , adversarial attack methods aim to create a minimally-perturbed input $\mathbf{x}' = \mathbf{x} + \delta$ that is mis-classified by the classifier either into a specific class (targeted attack) or into any class other than c (untargeted attack). This is formulated as an optimization problem, which in its most general form looks like

¹The code base associated with our work can be found at:
<https://github.com/jayaram-r/adversarial-detection>.

$$\begin{aligned} \min_{\delta} \quad & \|\delta\|_p \quad \text{s.t.} \\ & \hat{C}(\mathbf{x} + \delta) = c' \quad (\text{targeted}) \\ \text{or} \quad & \hat{C}(\mathbf{x} + \delta) \neq c \quad (\text{untargeted}) \end{aligned}$$

A number of adversarial attack methods have been proposed based on this general formulation [6, 13–16, 37–39]. Some of the well-known methods for generating adversarial data include the fast gradient sign method (FGSM) [13], projected gradient descent (PGD) attack [16], Carlini-Wagner attack [15], and DeepFool attack [37]. These attack methods can be categorized into *white-box* or *black-box* depending on the extent of their knowledge about the classifier’s structure, parameters, loss function, and learning algorithm. Most of the commonly used test-time attacks on DNN classifiers are strongly white-box in that they assume a complete knowledge of the system. For a detailed discussion and taxonomy of adversarial attack methods, we refer readers to the recent surveys [40, 41].

2.2 Adversarial Defenses

On the defense side of adversarial learning, the focus can be broadly categorized into (1) *adversarial training* - where the objective is to train robust classifiers that generalize well in the face of adversarial attacks [13, 16, 42, 43], (2) *adversarial detection* - where the objective is to detect inputs that are adversarially manipulated by identifying signatures or patterns that make them different from natural inputs seen by the classifier at training time [19, 20, 22, 23]. One approach to adversarial training involves augmenting the training set of the classifier with adversarial samples created from one or multiple attack methods along with their true labels, and retraining the classifier on the augmented training set (possibly initialized with parameters from a prior non-adversarial training) [13]. A limitation of this approach is that the resulting classifier may still fail on attacks that were not seen by the classifier during training. This has lead to research in the direction of robust optimization, where the learning objective of the classifier (usually an empirical risk function) is modified into a min-max optimization problem, with the inner maximization performed on a suitably chosen perturbation set (e.g., an l_∞ norm ball) [16]. Adversarial detection, on the other hand, does not usually involve special training or modification of the underlying classifier to predict accurately on adversarial inputs. Instead, the focus is on methods that can detect adversarial inputs while operating at low false positive (natural inputs detected as adversarial) rates using ideas from the anomaly detection literature. The detector flags inputs that are suspicious and likely to be misclassified by the classifier so that they may be analyzed by an expert (possibly another ML system) for decision making down the line. There have been a plethora of works on the defense side adversarial learning. Recent surveys on this topic can be found in [10, 44].

Adversarial Samples as Anomalies

Adversarial detection is closely related to the problem of anomaly or outlier detection [45, 46] with some important distinctions. The objective of anomaly detection is to determine if an input follows a pattern that is significantly different from that observed on a given data set. Stated differently, an input is said to be anomalous if it has a very low probability under the reference marginal distribution $p_0(\mathbf{x})$ underlying a given data set. On the other hand, adversarial inputs from a test-time attack are not necessarily anomalous with respect to the marginal data distribution because of the way they are created by minimally perturbing a valid input $\mathbf{x} \sim p_0(\cdot | c)$ from a given class c . It is useful to consider the following notion of adversarial inputs. Suppose a clean input \mathbf{x} from class c (i.e., $\mathbf{x} \sim p_0(\cdot | c)$) is perturbed to create an adversarial input \mathbf{x}' that appears to be from the same class c according to the true (Bayes) class posterior distribution, i.e., $c = \arg \max_k p_0(k | \mathbf{x}')$. However, it is predicted into a different class c' by the classifier, i.e., $\hat{C}(\mathbf{x}') = \arg \max_k F_k(\mathbf{x}') = c'$. From this standpoint, we hypothesize that an adversarial input \mathbf{x}' is likely to be a typical sample from the conditional distribution $p_0(\cdot | c)$ of the true class, while it is also likely to be an anomalous sample from the conditional distribution $p_0(\cdot | c')$ of the predicted class. We note that Miller *et al.* [28] use a similar hypothesis to motivate their detection method.

Supervised vs. Unsupervised Detection

It is useful to categorize adversarial detection methods into unsupervised or supervised based on whether they use adversarial data (from specific attack methods) for training and optimization. Supervised methods such as those in prior work [19, 22, 23, 29] usually train a binary classifier (e.g., logistic regression) to discriminate natural from adversarial inputs using data from specific

attack method(s), in some cases even tuning hyper-parameters using attack data. This raises the question of how well such methods can detect inputs from different attack methods not seen during training, including the case of an adaptive adversary that can intelligently select from a combination of strong attacks. Also, attack methods often have parameters that control their strength and success rate, *e.g.*, radius of the perturbation norm ball of FGSM and PGD [13, 16], or the confidence factor of the Carlini-Wagner attack [15]. Therefore, supervised methods have to be presented with a broad sampling of attack data, even from a single method, in order to generalize well to new attacks. On the other hand, unsupervised methods rely solely on patterns observed in a training set of clean (non-adversarial) data in order to identify test inputs that exhibit anomalous behaviour. Some recent works in adversarial detection that may be categorized as unsupervised include [21, 24, 26–28, 33].

2.3 Related Works

We categorize and review some prior works on adversarial and OOD detection. A more detailed survey and taxonomy of anomaly detection methods in deep learning can be found in [47].

Supervised Methods

In Lee *et al.* [22], the layer representations of a DNN are modeled class-conditionally using multi-variate Gaussian densities, which leads to the Mahalanobis distance from the mean vector as a layer feature. The feature vector of Mahalanobis distances from the layers is used to train a binary logistic classifier for discriminating adversarial (or OOD samples) from natural samples. Ma *et al.* [23] propose using the LID of layer representations of a DNN as a feature for characterizing adversarial samples. Similar to the approach of Lee *et al.* [22], they calculate a feature vector of LID estimates from the layer representations, which is used for training a logistic classifier for discriminating adversarial samples from natural samples. In Yang *et al.* [29], feature attribution methods are used to characterize the input and intermediate layer representations of a DNN. They find that adversarial inputs drastically alter the feature attribution map compared to natural inputs. Measures such as the inter-quartile range and median absolute deviation are used to quantify the dispersion in the distribution of attribution values, which are then used as features to train a logistic classifier for discriminating adversarial samples from natural samples.

Unsupervised Methods

Roth *et al.* [24] show that log-odds ratio of inputs to a classifier (not necessarily a DNN) can reveal some interesting properties of adversarial inputs. They propose a test statistic based on the expected log-odds of noise-perturbed inputs, which is thresholded to detect adversarial inputs. In Zheng *et al.* [26], the class-conditional distributions of fully-connected intermediate layer representations are modeled using Gaussian mixture models². Inputs with a likelihood lower than a (class-specific) threshold under each class-conditional mixture model are rejected as adversarial. In Miller *et al.* [28], an anomaly detection method focusing on adversarial attacks is proposed, which in its basic form can be described as follows. The class-conditional density of the layer representations of a DNN are modeled using Gaussian mixture models, and they are used to calculate a Bayes class posterior at each layer. The Kullback-Leibler divergence between the class posterior of the DNN (based on the softmax function) and the estimated Bayes class posterior from each layer are used as test statistics for detecting adversarial samples. A number of variations of this test statistic that lead to improved detection are also proposed. Sastry *et al.* [33] propose a method for detecting OOD samples based on analyzing the Gram matrices of the layer representations (activations) of a DNN. The Gram matrices of different orders (order 1 corresponds to the standard definition) capture the pairwise correlations between the elements of a layer activation. At training time, their detector records the element-wise minimum and maximum values of the Gram matrices (of different orders) from a training set of natural inputs, conditioned on each predicted class. The extent of deviation from the minimum and maximum values observed at training time is used to calculate a class-specific deviation test statistic at each layer. The final score for OOD detection is obtained by adding up the normalized deviations from the layers, where the normalization factor for a layer is the expected deviation observed on a held-out validation dataset³.

²Convolutional layers are not modeled in their approach.

³We note that the deviation statistic based on Gram matrices from the layer activations defined by [33] can be used as a test statistic for ReBeL as well. Different from [33], ReBeL would combine the layerwise, class-conditional p-values estimated from the test statistics into an adversarial score (§ 3.4) or OOD score (§ 3.5).

Confidence Metrics for Classifiers

Works such as the trust score [32] and deep KNN [27] have explored the problem of developing a confidence metric that can be used to independently validate the predictions of a classifier. Inputs with a low confidence score are expected to be mis-classified and can be flagged as potentially adversarial or OOD. The deep KNN method [27] uses the class labels of the k-nearest neighbors of DNN layer representations to calculate a non-conformity score corresponding to each class. Large values of non-conformity corresponding to the predicted class indicate that an input may not have a reliable prediction. The method calculates empirical p-values of the non-conformity scores to provide a confidence score, credibility score, and an alternate (corrected) class prediction for test inputs. The trust score [32] estimates the α -high density (level) set for each class, and calculates the distances from a test point to the α -high density sets from the classes to define a confidence metric. These methods can also be categorized as unsupervised.

3 Proposed Method

A high-level overview of our proposed framework for detecting anomalous inputs is given in Fig. 1. We first introduce some notations and provide an overview of the problem and our solution approach.

Notations and Definitions: Consider the conventional classification problem where the goal is to accurately classify an input $\mathbf{x} \in \mathcal{X}$ into one of m classes $[m] := \{1, \dots, m\}$. We focus on DNN classifiers that learn a function of the form $\mathbf{F}(\mathbf{x}) = [F_1(\mathbf{x}), \dots, F_m(\mathbf{x})] : \mathcal{X} \mapsto \Delta_m$, where \mathcal{X} is the space of inputs to the DNN (e.g., $[0, 255]^{3hw}$ for a $h \times w$ color image) and $\Delta_m = \{(p_1, \dots, p_m) \in [0, 1]^m \mid \sum_i p_i = 1\}$ is the $m-1$ probability simplex to which the output class probabilities are constrained. The multi-layer architecture of a DNN allows the input-output mapping to be expressed as a composition of multiple functions, i.e., $\mathbf{F}(\mathbf{x}) = (\mathbf{g}_L \circ \mathbf{g}_{L-1} \cdots \circ \mathbf{g}_1)(\mathbf{x})$, where L is the number of layers. The outputs from an intermediate layer $i \in \{1, \dots, L\}$ of the DNN $\mathbf{f}_i(\mathbf{x}) = (\mathbf{g}_i \circ \dots \circ \mathbf{g}_1)(\mathbf{x}) \in \mathbb{R}^{d_i}$ are referred to as its layer representations (or layer activations)⁴. We also use the shorthand notation $\mathbf{x}^{(i)} := \mathbf{f}_i(\mathbf{x})$ for the i -th layer representation of an input \mathbf{x} , with $\mathbf{f}_0(\mathbf{x}) = \mathbf{x}^{(0)} := \mathbf{x}$ denoting the input for convenience. The decision rule of the classifier is to predict the class corresponding to the maximum of its output confidence scores, $\hat{C}(\mathbf{x}) = \arg \max_{c \in [m]} F_c(\mathbf{x})$. Table 1 provides a quick reference for the terms used in the paper.

| Term | Description |
|--|--|
| $\mathcal{X} \subset \mathbb{R}^{d_0}$ | Space of inputs to the DNN. |
| $\Delta_m = \{(p_1, \dots, p_m) \in [0, 1]^m \mid \sum_i p_i = 1\}$ | Space of output probabilities from the m classes. |
| $\mathbf{F}(\mathbf{x}) = [F_1(\mathbf{x}), \dots, F_m(\mathbf{x})] : \mathcal{X} \mapsto \Delta_m$ | Input-output mapping learned by the DNN. |
| $\hat{C}(\mathbf{x}) = \arg \max_{i \in [m]} F_i(\mathbf{x})$ | Class prediction of the DNN. |
| $\mathbf{x}^{(i)} := \mathbf{f}_i(\mathbf{x}) \in \mathbb{R}^{d_i}, i = 0, 1, \dots, L$ | Flattened layer representations of the DNN; index 0 is used for the input. |
| C and \hat{C} | Random variables corresponding to the true class and DNN-predicted class. |
| $\mathcal{D}_a = \{(\mathbf{x}_n^{(0)}, \dots, \mathbf{x}_n^{(L)}, c_n, \hat{c}_n), n = \{1, \dots, N\}\}$ | Labeled dataset with the layer representations, true class, and predicted class. |
| $T_p(\mathbf{x}^{(l)}, \hat{c}) := T_{p \hat{c}}^{(l)}$ | Test statistic from layer l conditioned on the predicted class \hat{c} . |
| $T_s(\mathbf{x}^{(l)}, c) := T_{s c}^{(l)}$ | Test statistic from layer l conditioned on the candidate true class c . |
| $\mathbf{t}_{p \hat{c}} := [t_{p \hat{c}}^{(0)}, \dots, t_{p \hat{c}}^{(L)}]$ | Vector of test statistics from the layers conditioned on the predicted class \hat{c} . |
| $\mathbf{t}_{s c} := [t_{s c}^{(0)}, \dots, t_{s c}^{(L)}]$ | Vector of test statistics from the layers conditioned on the candidate true class c . |
| $q_*(\mathbf{t}_{p \hat{c}})$ | Combined p-value of the test statistics conditioned on the predicted class \hat{c} . |
| $q_*(\mathbf{t}_{s c})$ | Combined p-value of the test statistics conditioned on the candidate true class c . |
| $(k_1^{(l)}, \dots, k_m^{(l)}) \in \{0, 1, \dots, k\}^m$ s.t. $\sum_i k_i^{(l)} = k$ | Class counts from the k -nearest neighbors of a representation vector from layer l . |
| $\ \cdot\ _p$ | l_p norm of a vector. |
| $d(\mathbf{x}, \mathbf{y})$ | Distance between a pair of vectors; cosine distance unless specified otherwise. |

Table 1: Notations and Definitions

3.1 Approach Overview

Given a test sample \mathbf{x} whose true class c is unknown, we observe its DNN-predicted class $\hat{C}(\mathbf{x}) = \hat{c}$ and representations from selected layers $\mathbf{x}^{(l)}, l = 0, 1, \dots, L$. In the most general form, we would like to design a decision rule of the form

⁴Layers with tensor-valued outputs (e.g., convolution) are assumed to be flattened into vectors. Boldface symbols are used for vectors and matrices.

$$\delta(\mathbf{x}^{(0)}, \dots, \mathbf{x}^{(L)}, \hat{c}) = \begin{cases} 1 & \text{if } S(\mathbf{x}^{(0)}, \dots, \mathbf{x}^{(L)}, \hat{c}) \geq \tau \\ 0 & \text{otherwise} \end{cases} \quad (1)$$

where $S(\mathbf{x}^{(0)}, \dots, \mathbf{x}^{(L)}, \hat{c})$ is the decision statistic or score that is thresholded to decide if a test sample is anomalous (1) or natural (0). We assume access to a labeled data set $\mathcal{D} = \{(\mathbf{x}_n, c_n), n = 1, \dots, N\}$ that is different from the one used to train the DNN, and that does not contain any anomalous samples. We define an augmented data set $\mathcal{D}_a = \{(\mathbf{x}_n^{(0)}, \dots, \mathbf{x}_n^{(L)}, c_n, \hat{c}_n), n = 1, \dots, N\}$ that is obtained by passing samples from \mathcal{D} through the DNN and extracting their layer-wise representations and predicted class $\hat{C}(\mathbf{x}_n) = \hat{c}_n$. Instead of directly using the high-dimensional input and layer representations, we calculate a test statistic at each layer l (including the input) conditioned on the predicted class $T_p(\mathbf{x}^{(l)}, \hat{c})$ that captures how anomalous that layer's representation $\mathbf{x}^{(l)}$ is with respect to the distribution of natural inputs classified into the same class \hat{c} . Since the true class of an input is unknown at test time, we also calculate a test statistic at each layer l conditioned on each candidate value of the true class, $T_s(\mathbf{x}^{(l)}, c)$, $c \in [m]$. This test statistic captures how anomalous $\mathbf{x}^{(l)}$ is with respect to the distribution of natural inputs from the class c .

We propose to use test statistics that are a function of the samples within a small neighborhood of a DNN layer representation that capture a local statistical property relative to the class-conditional distribution of natural inputs (*e.g.*, the average distance from a layer representation to its k -nearest neighbors from a given class). We do not impose any constraint on the test statistic other than a basic requirement that larger values of the test statistic correspond to a higher level of nonconformity relative to the distribution of natural inputs. When clear from the context, we use the shorthand notation $T_p^{(l)}$ and $T_s^{(l)}$ to denote the random variables, and $t_p^{(l)}$ and $t_s^{(l)}$ to denote specific values of the class-conditional test statistics from layer l .

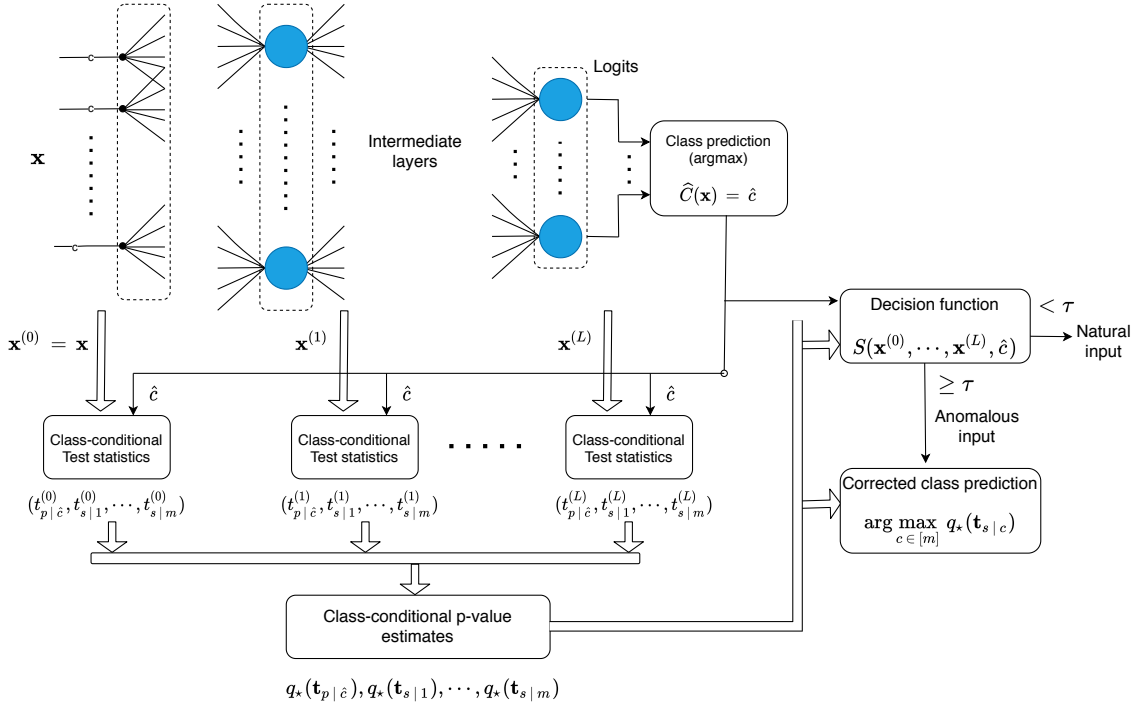


Figure 1: Overview of the proposed detection framework. The DNN classifies a test input \mathbf{x} into one of the m classes. ReBeL uses the predicted class and the layer representations to calculate class-conditional test statistics at each layer. The class-conditional test statistics from the layers are combined into class-conditional p-value estimates, which are then used by the decision function to determine whether the input is natural or anomalous. ReBeL also provides a corrected prediction for the true class of the input, which is useful when the input is detected as adversarial.

Problem Statement: Given a vector of test statistics from the layers $\mathbf{t}_{p|\hat{c}} := [t_{p|\hat{c}}^{(0)}, \dots, t_{p|\hat{c}}^{(L)}]$ conditioned on the predicted class \hat{c} , and a vector of test statistics from the layers $\mathbf{t}_{s|c} := [t_{s|c}^{(0)}, \dots, t_{s|c}^{(L)}]$ conditioned on each candidate true class c , we would like to design a detection rule of the form Eq. (1) in order to determine if the test statistics are jointly distributed according to the null hypothesis (of natural inputs) or the alternative (of anomalous inputs).

Towards this end, we first propose an approach that is based on combining p-values estimated at each individual layer from the univariate class-conditional distribution of the test statistics. In scenarios where the number of layers is not large, we include additional p-values estimated from the bivariate class-conditional distribution of test statistics from all distinct layer pairs. The motivation is that anomalous inputs are likely to produce distinct patterns at one or more layer representations that can be detected using the p-values at the layers and layer pairs. We propose a second approach that is based on considering jointly the vector of test statistics from the layers, and estimating their multivariate p-values using a non-parametric p-value estimation method from the anomaly detection literature [46, 48]. In contrast to the first approach, here we implicitly consider the class-conditional, joint distribution of the test statistics to estimate a single p-value across the layers.

3.2 Testing At Individual Layers & Layer Pairs

The p-value is widely used in hypothesis testing to evaluate how extreme an observed sample is with respect to the null hypothesis distribution, with smaller values corresponding to stronger evidence that the null hypothesis is not true [49]. Suppose the test statistic for an input at layer l relative to the predicted class \hat{c} is $t_{p|\hat{c}}^{(l)}$, and the test statistic relative to each candidate source (true) class $c \in [m]$ is $t_{s|c}^{(l)}$, then the p-values corresponding to the test statistics are defined for the predicted and each candidate source class respectively as follows:⁵

$$\begin{aligned} q(t_{p|\hat{c}}^{(l)}) &:= \Pr[T_{p|\hat{c}}^{(l)} \geq t_{p|\hat{c}}^{(l)} | \hat{C} = \hat{c}] \\ q(t_{s|c}^{(l)}) &:= \Pr[T_{s|c}^{(l)} \geq t_{s|c}^{(l)} | C = c], \quad c = 1, \dots, m. \end{aligned} \quad (2)$$

It is straightforward to extend the above definitions for (one-sided, right-tailed) p-values at a pair of layers l_1 and l_2 conditioned on the predicted class $q(t_{p|\hat{c}}^{(l_1)}, t_{p|\hat{c}}^{(l_2)})$, and each candidate true class $q(t_{s|c}^{(l_1)}, t_{s|c}^{(l_2)}), \forall c \in [m]$. These p-values can, in principle, be calculated for all distinct layer pairs. However, we recommend including them only when L is small both for computational reasons, and in order to control the false positive rate (FPR) that could result from a large number of comparisons. Since the class-conditional distribution of the test statistics is usually unknown, the p-values can be estimated using the empirical cumulative distribution function of the test statistics observed from a data sample following the null distribution, with larger samples leading to more accurate estimates⁶.

In the single hypothesis test setting, the standard approach is to compare the p-value to a specific significance level (e.g., 0.01) and reject the null hypothesis when the p-value is smaller than that level [49]. When multiple tests on the same hypothesis are involved, as in the above problem, rejecting the null hypothesis based on comparing the p-values to a single significance level can lead to an increasing FPR as the number of comparisons increases [51]. With the goal of formulating a scoring function for anomaly detection, we investigate two methods for combining p-values from multiple tests, viz. Fisher’s method [52] and the harmonic mean p-value (HMP) method [53]. To maintain clarity, we only describe Fisher’s method here and describe the HMP method in Appendix A.

Combining p-values from multiple tests: The Fisher’s method provides a principled way of combining p-values from multiple independent hypothesis tests based on the idea that, under the null hypothesis, each p-value is uniformly distributed in $[0, 1]$, and the sum of log of multiple p-values follows a χ^2 distribution [52]. In our problem, the log of the combined p-value from multiple layers and layer pairs, conditioned on the predicted class and on each candidate true class are given respectively by,

⁵We use one-sided, right-tailed p-values because of the way the test statistics are defined.

⁶We calculate the average p-value from a hundred bootstrap samples in order to reduce the variance. Alternatively, techniques such as KDE [50] can be used for obtaining smoothed estimates of the p-value.

$$\begin{aligned}
\log q_{\text{fis}}(\mathbf{t}_{p|\hat{c}}) &= \sum_{l=0}^L \log q(t_{p|\hat{c}}^{(l)}) + \sum_{\substack{l_1, l_2 \in [L]^2 \\ l_2 > l_1}} \log q(t_{p|\hat{c}}^{(l_1)}, t_{p|\hat{c}}^{(l_2)}) \\
\log q_{\text{fis}}(\mathbf{t}_{s|c}) &= \sum_{l=0}^L \log q(t_{s|c}^{(l)}) + \sum_{\substack{l_1, l_2 \in [L]^2 \\ l_2 > l_1}} \log q(t_{s|c}^{(l_1)}, t_{s|c}^{(l_2)}), \quad \forall c \in [m]. \quad (3)
\end{aligned}$$

3.3 Joint Multivariate Testing Of All The Layers

In contrast to the method in § 3.2, here we consider the joint class-conditional distribution of the test statistics from the layers and estimate a multivariate p-value for a test input. The idea of a multivariate p-value can be understood in terms of level sets of the joint density of the test statistics under the null hypothesis of natural inputs. Consider an input predicted into a class \hat{c} , that has a vector of test statistics $\mathbf{t}_{p|\hat{c}}^*$ from the layers. Suppose $f_0(\mathbf{t}_{p|\hat{c}}|\hat{c})$ denotes the true (unknown) density of the test statistics conditioned on the predicted class \hat{c} , then the region outside the level set of constant density equal to $f_0(\mathbf{t}_{p|\hat{c}}^*|\hat{c})$ is given by $\{\mathbf{t}_{p|\hat{c}} : f_0(\mathbf{t}_{p|\hat{c}}|\hat{c}) < f_0(\mathbf{t}_{p|\hat{c}}^*|\hat{c})\}$. The multivariate p-value for $\mathbf{t}_{p|\hat{c}}^*$ is the probability of this region under the null hypothesis measure [46, 48].

We use the averaged localized p-value estimation method using kNN graphs (aK-LPE) proposed by Qian *et al.* [48], which is an extension of earlier work [46]. The main idea is to define a score function based on the distances of a test point to its k-nearest neighbors (kNN) that acts as a surrogate function capturing the local relative density at the test point. They show that a score function $G(\mathbf{x})$ defined as the average distance from a point \mathbf{x} to its $\frac{k}{2}$ -th nearest neighbor and $\frac{3k}{2}$ -th nearest neighbor can provide an asymptotically-consistent p-value estimator. In our problem, we apply the aK-LPE method on the vector of test statistics conditioned on the predicted class to estimate the p-value $q_{\text{lpe}}(\mathbf{t}_{p|\hat{c}})$. Likewise, we apply the method on the vector of test statistics conditioned on each candidate source class to estimate the p-values $q_{\text{lpe}}(\mathbf{t}_{s|c})$, $\forall c \in [m]$. We note that this method requires a large number of null-distribution samples in order to provide reliable p-value estimates.

3.4 Scoring For Adversarial Sample Detection

We have all the components required to define the scoring function for adversarial detection in Eq. (1). First, consider the hypothesis that an adversarial input predicted into a class \hat{c} by the DNN is likely to be anomalous at one or more of its layer representations relative to the distribution of natural inputs predicted into the same class \hat{c} . This implies that the p-value of the test statistics conditioned on the predicted class, $q_*(\mathbf{t}_{p|\hat{c}})$ ⁷, should have a small value. Moreover, since the adversarial input was created from a source class different from \hat{c} , it is likely to be a typical sample relative to the distribution of natural inputs from the unknown source class $c \neq \hat{c}$. This implies that the p-value of the test statistics conditioned on one of the candidate true classes, $q_*(\mathbf{t}_{s|c})$, $c \in [m] \setminus \{\hat{c}\}$, should have a relatively large value. Combining these ideas, the score function for adversarial detection for an input with predicted class \hat{c} is given by

$$S(\mathbf{x}^{(0)}, \dots, \mathbf{x}^{(L)}, \hat{c}) = \frac{\max_{c \in [m] \setminus \{\hat{c}\}} q_*(\mathbf{t}_{s|c})}{q_*(\mathbf{t}_{p|\hat{c}})}. \quad (4)$$

This score function can be used with any of the methods defined earlier for estimating the combined or multivariate p-value from the layers. It is instructive to consider the numerator and denominator of the score in the following three cases. 1) For correctly classified inputs, the numerator is expected to be small and the denominator is expected to be large, resulting in a low score overall. 2) For misclassified natural inputs, both the numerator and denominator are expected to be large, resulting in a mid-range score. 3) For adversarial inputs, the numerator is expected to be large and the denominator is expected to be small, resulting in a higher score compared to the other cases.

3.5 Scoring For Out-Of-Distribution Sample Detection

OOD inputs are similar to adversarial inputs in that they are also likely to exhibit anomalous patterns at one or more layers of the DNN relative to the distribution of natural inputs with the same predicted

⁷We use the notation $q_*(\cdot)$ to denote one of the possible p-value functions $q_{\text{fis}}(\cdot)$, $q_{\text{hmp}}(\cdot)$, and $q_{\text{lpe}}(\cdot)$.

class. However, an OOD input is not created by intentionally perturbing a natural input with true class different from the predicted class. Therefore, we modify the score function in Eq. (4) for OOD detection by including only the denominator term, *i.e.*,

$$S_{\text{ood}}(\mathbf{x}^{(0)}, \dots, \mathbf{x}^{(L)}, \hat{c}) = q_{\star}(\mathbf{t}_p | \hat{c})^{-1}. \quad (5)$$

Anomalous inputs are expected to have a low p-value under the class predicted by the DNN, and hence a high value for the above score ⁸.

3.6 Correcting The Classifier's Prediction

The detector defined in Eq. (1) can be used to monitor test inputs to a DNN and flag inputs that score above a threshold as potentially adversarial. Given a target FPR of $\alpha \in (0, 1)$ (usually a small value *e.g.*, 0.01), the threshold can be tuned by estimating the FPR on a set of natural inputs as

$$\tau_{\alpha} = \sup\{\tau \geq 0 : \hat{P}_{\text{F}}(\tau) \leq \alpha\}; \quad \hat{P}_{\text{F}}(\tau) = \frac{1}{N} \sum_{n=1}^N \mathbb{1}(S(\mathbf{x}_n^{(0)}, \dots, \mathbf{x}_n^{(L)}, \hat{c}_n) \geq \tau), \quad (6)$$

where $\mathbb{1}(\cdot)$ is the indicator function taking value 1 when its input condition is satisfied. The classifier provides its prediction when the detection score on an input is below the threshold; this accounts for a vast majority ($1 - \alpha$ fraction) of natural inputs. For inputs that score above the threshold (*i.e.*, detected as adversarial), we propose to use the class corresponding to the maximum (combined or multivariate) p-value of the test statistics, conditioned on each candidate source class, as the corrected class prediction. The combined classification rule of the DNN and the detector is ⁹:

$$\hat{C}_{\text{comb}}(\mathbf{x}) = \begin{cases} \hat{C}(\mathbf{x}) & \text{if } S(\mathbf{x}^{(0)}, \dots, \mathbf{x}^{(L)}, \hat{c}) < \tau_{\alpha} \\ \arg \max_{c \in [m]} q_{\star}(\mathbf{t}_s | c) & \text{otherwise} \end{cases} \quad (7)$$

3.7 Test Statistics At The DNN Layers

We propose a specific test statistic that captures how well the class counts among the k-nearest neighbors (kNN) of a layer representation of the DNN follow the expected multinomial class count distributions estimated from a training set of natural samples. Our experimental results in the main paper are based on the multinomial test statistic. We present additional methods for calculating test statistics in Appendix B, and experimentally compare the performance of ReBeL using different test statistics in Appendix E.5. Recall that $\mathcal{D}_a = \{(\mathbf{x}_n^{(0)}, \dots, \mathbf{x}_n^{(L)}, c_n, \hat{c}_n), n \in [N]\}$ is a set of labeled samples augmented with the DNN layer representations and the predicted class. The index set of the k -nearest neighbors of a layer representation $\mathbf{x}^{(l)} \in \mathbb{R}^{d_l}$ relative to the dataset \mathcal{D}_a is denoted by $N_k^{(l)}(\mathbf{x}^{(l)}, \mathcal{D}_a) \subset [N]$. For brevity, we drop \mathcal{D}_a from the notation when it is clear from the context.

Multinomial class count based test statistic

If we consider a set of natural inputs to the DNN that are predicted into a class \hat{c} , the distribution of class counts from the kNN of its layer representations may be expected to follow a certain distribution that has a higher probability for class \hat{c} than the rest. This observation can also be applied to the natural inputs from a given true class c . Let $(k_1^{(l)}, \dots, k_m^{(l)})$ denote the tuple of class counts from the kNN $N_k^{(l)}(\mathbf{x}^{(l)})$ of a layer representation $\mathbf{x}^{(l)}$ such that $k_i^{(l)} \in \{0, 1, \dots, k\}$ and $\sum_i k_i^{(l)} = k$. The natural or null distribution of the kNN class counts at a layer l conditioned on a predicted class \hat{c} can be captured by the following multinomial distribution

$$p(k_1^{(l)}, \dots, k_m^{(l)} | \hat{C} = \hat{c}) = k! \prod_{i=1}^m \frac{[\pi_i^{(l)} | \hat{c}]^{k_i^{(l)}}}{k_i^{(l)}!}, \quad (8)$$

where $(\pi_1^{(l)} | \hat{c}, \dots, \pi_m^{(l)} | \hat{c})$ are multinomial probability parameters (specific to class \hat{c} and layer l) that are constrained to lie in the $m-1$ probability simplex Δ_m . These parameters, although unknown, can

⁸In practice, we compute the natural log of the scores in Eq. (4) and Eq. (5) for numerical stability.

⁹This is not applicable to general anomalous inputs since they may not be from the predefined set of classes.

be estimated from the labeled subset of \mathcal{D}_a predicted into class \hat{c} , $\{(\mathbf{x}_n^{(0)}, \dots, \mathbf{x}_n^{(L)}, c_n, \hat{c}_n), n = 1, \dots, N \mid \hat{c}_n = \hat{c}\}$, using the framework of maximum likelihood or maximum-a-posteriori (MAP) estimation. We use MAP estimation with the Dirichlet conjugate prior distribution [54] and hyper-parameters (prior count from each class) set to a small nonzero value in order to avoid 0 estimates for the probability parameters.

If a test input \mathbf{x} , classified into class \hat{c} by the DNN, follows the natural data distribution, we would expect distribution Eq.(8) to be a good fit for the class counts observed from its kNN at layer l . A well-known goodness-of-fit test for the multinomial distribution is the likelihood ratio test (LRT), which computes a log likelihood ratio as the test statistic [55]. In order to test whether the observed class counts $(k_1^{(l)}, \dots, k_m^{(l)})$ from layer l , given predicted class \hat{c} , is consistent with distribution (8), the LRT test statistic is given by

$$T_p(\mathbf{x}^{(l)}, \hat{c}) = \sum_{i=1}^m k_i^{(l)} \log \frac{k_i^{(l)}}{k \pi_{i|\hat{c}}^{(l)}}. \quad (9)$$

This test statistic is always non-negative, with larger values corresponding to a larger deviation from the null distribution Eq.(8).

In a similar way, the natural or null distribution of the kNN class counts at a layer l conditioned on a true class c can be captured by the following multinomial distribution

$$p(k_1^{(l)}, \dots, k_m^{(l)} \mid C = c) = k! \prod_{i=1}^m \frac{[\tilde{\pi}_i^{(l)}]^{k_i^{(l)}}}{k_i^{(l)}!}. \quad (10)$$

The LRT test statistic corresponding to this multinomial distribution is given by

$$T_s(\mathbf{x}^{(l)}, c) = \sum_{i=1}^m k_i^{(l)} \log \frac{k_i^{(l)}}{k \tilde{\pi}_{i|c}^{(l)}}. \quad (11)$$

Since the true class of a test input is unknown, we calculate this test statistic for each candidate true class $c \in [m]$. Although we use the LRT test statistic as a class count deviation measure, we do not rely on its asymptotic properties such as convergence to the χ^2 distribution (when scaled by the factor -2), which would not be applicable in our scenario where k is a small integer.

4 Defense-Aware Custom Attack

The importance of evaluating an adversarial detection method against an adaptive, defense-aware adversary has been highlighted in prior works [30, 31, 56]. We consider a gray-box adversary that is assumed to have full knowledge of the DNN architecture and parameters, and partial knowledge of our detection method¹⁰. The adversary can utilize this knowledge to create adversarial samples that attempt to simultaneously induce mis-classifications in the DNN and evade the detection method. Towards this end, we formulate a differentiable loss function along the lines of prior work [15, 57] that uses the input and internal layer representations of the DNN to create adversarial samples.

Consider a clean input sample \mathbf{x} from class c that is correctly classified by the DNN. Let η_l denote the distance between $\mathbf{x}^{(l)} = \mathbf{f}_l(\mathbf{x})$ (the l -th layer representation of \mathbf{x}) and its k -th nearest neighbor from layer l . The number of samples from any class i among the k -nearest neighbors of $\mathbf{x}^{(l)}$, relative to the labeled dataset \mathcal{D}_a , can be expressed as

$$k_i^{(l)} = \sum_{n=1: c_n=i}^N s(\eta_l - d(\mathbf{f}_l(\mathbf{x}), \mathbf{f}_l(\mathbf{x}_n))), \quad i = 1, \dots, m, \quad (12)$$

where $s(\cdot)$ is the unit step function. Consider the following probability mass function over the class labels: $p_i = k_i / \sum_{j=1}^m k_j$, $i \in [m]$, where $k_i = \sum_{l=0}^L k_i^{(l)}$ is the kNN count corresponding to class i summed over the layers. In order to fool defense methods relying on the kNN class counts from the layer representations, our attack attempts to find an adversarial input $\mathbf{x}' = \mathbf{x} + \zeta$ with target class $c' \neq c$ that minimizes the following log-ratio of probabilities:

¹⁰For example, the detection threshold and specific layers of the DNN used may be unknown.

$$\log \frac{p_c}{p_{c'}} = \log k_c - \log k_{c'} = \log \sum_{l=0}^L k_c^{(l)} - \log \sum_{l=0}^L k_{c'}^{(l)}, \quad (13)$$

subject to a penalty on the norm of the perturbation ζ . To address the non-smoothness arising from the step function in the class counts, we use the Gaussian (RBF) kernel $r(\mathbf{x}, \mathbf{y}, \sigma) = e^{-\frac{1}{\sigma^2} d(\mathbf{x}, \mathbf{y})^2}$ to obtain a smooth approximation of the class counts in Eq.(12)¹¹. The attack objective function to minimize is obtained by combining the kernel-smoothed log-ratio of probabilities with a penalty on the l_2 norm of the perturbation, *i.e.*,

$$J(\zeta) = \|\zeta\|_2^2 + \lambda \log \sum_{l=0}^L \sum_{\substack{n=1: \\ c_n=c}}^N r(\mathbf{f}_l(\mathbf{x} + \zeta), \mathbf{f}_l(\mathbf{x}_n), \sigma_l^2) - \lambda \log \sum_{l=0}^L \sum_{\substack{n=1: \\ c_n=c'}}^N r(\mathbf{f}_l(\mathbf{x} + \zeta), \mathbf{f}_l(\mathbf{x}_n), \sigma_l^2), \quad (14)$$

where $\sigma_l > 0$ is the scale of the kernel for layer l and $\lambda > 0$ is a constant that sets the relative importance of the terms in the objective function. Details of the optimization method and the choice of λ can be found in Appendix D.5. The method used for setting the kernel scale per layer and minor extensions of the proposed attack can be found in Appendix C. In our experiments, we choose the class with the second highest probability predicted by the DNN as the target attack class.

5 Experimental Results

We evaluated ReBeL on the following well-known image classification datasets: CIFAR-10 [59], SVHN [60], and MNIST [61]. We used the training partition provided by the datasets for training standard CNN architectures. We perform class-stratified 5-fold cross validation on the test partition provided by the datasets; the training folds are used for estimating the detector parameters, and the test folds are used solely for calculating performance metrics (which are averaged across the test folds). We used the Foolbox library [62] for generating adversarial samples from the following attack methods: (i) Projected Gradient Descent (PGD) with l_∞ norm [16], (ii) Carlini-Wagner (CW) attack with l_2 norm [15], and (iii) Fast gradient sign method (FGSM) with l_∞ norm [13]. We also implement and generate adversarial samples from the custom attack proposed in § 4. More details on the datasets, DNN architectures, and the attack parameters used are provided in Appendix D. Due to space constraints, we omit the results related to MNIST and FGSM, and present them in Appendix E.

We compare the performance of ReBeL (using Fisher’s method and the aK-LPE method combined with the multinomial test statistic) against the following recently proposed methods for adversarial and OOD detection: (i) Deep Mahalanobis detector (Mahalanobis) [22], (ii) Local Intrinsic Dimensionality detector (LID) [23], (iii) The odds are odd detector (Odds) [24], (iv) Deep kNN (DKNN) [27], and (v) Trust Score (Trust) [32]. Mahalanobis and LID methods are supervised (they utilize adversarial or outlier data from the training folds), while the remaining methods are unsupervised. LID and Odds are excluded from the OOD detection experiment because they specifically address adversarial samples. Details on the implementation, hyper-parameters, and layer representations used by the methods can be found in Appendix D.4.

We evaluate detection performance using the precision-recall (PR) curve [63, 64] and the receiver operating characteristic (ROC) curve [65, 66]. We use average precision as a threshold-independent metric to summarize the PR curve, and partial area under the ROC curve below FPR α (pAUC- α) as the metric to summarize low-FPR regions of the ROC curve.

5.1 Detecting Adversarial Samples

Figures 2 and 3 plot the average precision of the detection methods as a function of the perturbation l_2 norm of the adversarial samples generated from the CW and Custom attack methods. For the PGD attack, the proportion of adversarial samples is shown instead of the perturbation norm because most of the samples produced by this attack have the same norm value. We observe that across (almost) all cases, ReBeL outperforms the other baselines. Methods such as Mahalanobis, Odds, and DKNN perform well in some cases but fail on others, while LID performs poorly in nearly all scenarios. We observe an outlying trend in Figure 3b, where Odds outperforms ReBeL on the custom attack applied

¹¹ A similar approach has been used, *e.g.*, in the soft nearest-neighbor loss function [58].

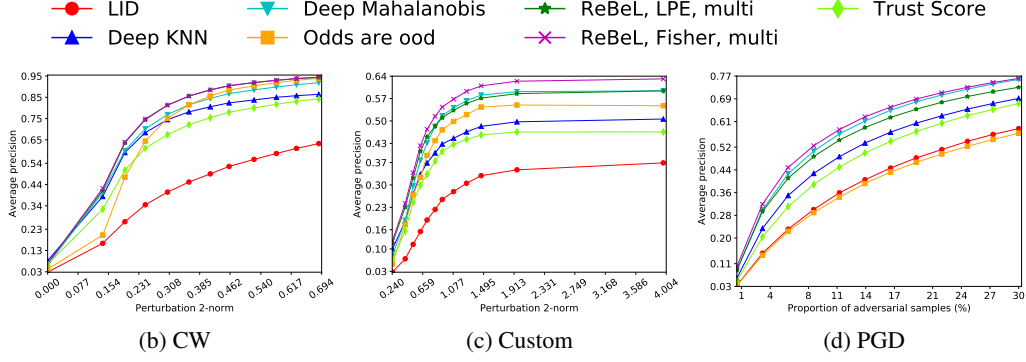


Figure 2: Adversarial detection performance on CIFAR-10.

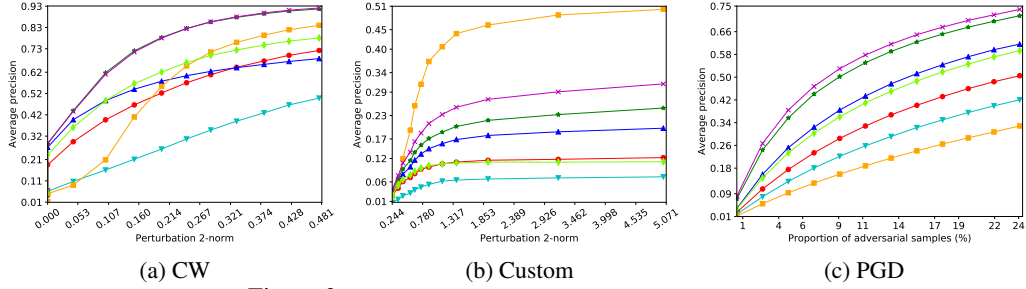


Figure 3: Adversarial detection performance on SVHN.

to SVHN. However, a comparison of the pAUC-0.2 metric (Figure 7 in Appendix E.2) for this scenario reveals that ReBeL has higher pAUC-0.2 for low perturbation norm (where adversarial samples are likely to be more realistic and harder to detect). We provide additional results in Appendix E that include: (i) evaluation of the pAUC-0.2 metric, (ii) results on MNIST, and (iii) results on FGSM.

5.2 Detecting Out-Of-Distribution Samples

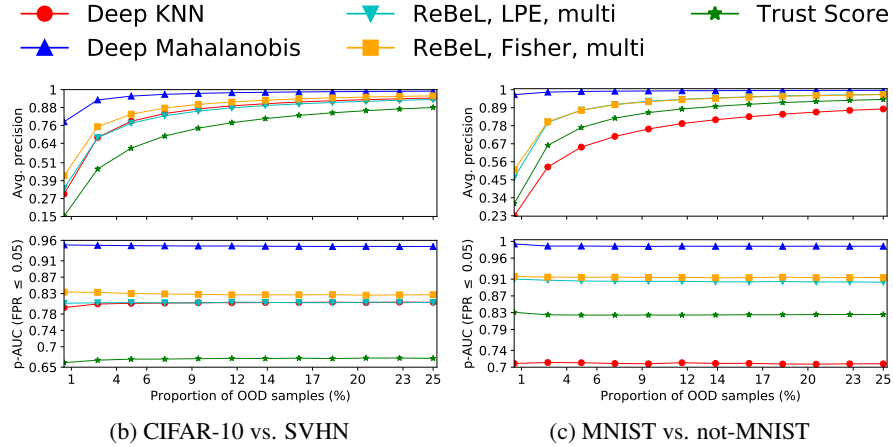


Figure 4: OOD detection performance.

Figures 4b and 4c compare the performance of ReBeL with Mahalanobis, DKNN, and Trust on two OOD detection tasks. Details of the experimental setup are provided in Appendix D.3. The plots show average precision and pAUC-0.05 as a function of the proportion of OOD samples¹². Observe that ReBeL outperforms the unsupervised methods DKNN and Trust in both cases, but does not achieve

¹²We report pAUC below 5% FPR because the methods achieve high detection rates at very low FPR.

the near-perfect performance of Mahalanobis. Note that Mahalanobis is a supervised method that uses outlier samples from the training folds to train a classifier and tune a noise parameter [22]. However, in real-world settings, it is unlikely that one would have prior knowledge or sufficient number of outlier samples for training.

5.3 Corrected Classification Performance

In Table 2, we present the accuracy of the combined classification rule proposed in § 3.6 (with Fisher’s method and the multinomial test statistic) compared against the corrected class prediction of DKNN [27] on both clean data and adversarial data generated using the CW attack. The detection threshold is set using Eq. (6) for target FPRs of 0.5% and 2%. We observe that ReBeL achieves a reasonable accuracy in most cases, which is notable because the accuracy of the DNN would be close to 0 without any defense mechanism. Also, ReBeL significantly outperforms DKNN in all cases.

| Dataset | Method | Accuracy (%), Clean data | | Accuracy (%), CW, confidence = 0 | | Accuracy (%), CW, confidence = 6 | | Accuracy (%), CW, confidence = 14 | |
|----------|----------|-----------------------------|----------------|-------------------------------------|----------------|-------------------------------------|----------------|--------------------------------------|----------------|
| | | $\alpha = 0.5\%$ | $\alpha = 2\%$ | $\alpha = 0.5\%$ | $\alpha = 2\%$ | $\alpha = 0.5\%$ | $\alpha = 2\%$ | $\alpha = 0.5\%$ | $\alpha = 2\%$ |
| CIFAR-10 | ReBeL | 95.01 | 94.93 | 47.57 | 52.67 | 22.39 | 26.51 | 25.24 | 28.41 |
| | Deep kNN | 95.47 | 95.40 | 1.78 | 19.54 | 0.46 | 6.38 | 0.74 | 8.56 |
| SVHN | ReBeL | 89.79 | 90.12 | 45.72 | 63.26 | 33.53 | 47.36 | 39.16 | 56.19 |
| | Deep kNN | 89.46 | 89.57 | 0.22 | 1.25 | 0.22 | 1.37 | 0.23 | 1.57 |
| MNIST | ReBeL | 98.94 | 98.84 | 87.02 | 88.86 | 80.21 | 82.64 | 84.89 | 86.74 |
| | Deep kNN | 99.01 | 98.66 | 1.05 | 4.54 | 1.14 | 5.23 | 1.12 | 4.93 |

Table 2: Corrected classification performance of ReBeL and DKNN.

6 Conclusion

We presented ReBeL, an unsupervised framework for detecting anomalous inputs to a DNN classifier that is based on joint statistical testing of the DNN layer representations. We proposed specialized scoring methods for detecting adversarial and OOD inputs. In the case of adversarial inputs, we also proposed an effective method for correcting the class prediction of the DNN. The construction of ReBeL is modular, allowing it to be used with a variety of test statistics calculated at the DNN layers. Through extensive experiments with strong adversarial attacks and anomalous inputs to DNN image classifiers, we have shown that ReBeL outperforms several recent competing methods.

References

- [1] Kaiming He, Xiangyu Zhang, Shaoqing Ren, and Jian Sun. Delving deep into rectifiers: Surpassing human-level performance on imagenet classification. In *2015 IEEE International Conference on Computer Vision, ICCV 2015, Santiago, Chile, December 7-13, 2015*, pages 1026–1034. IEEE Computer Society, 2015.
- [2] Alex Krizhevsky, Ilya Sutskever, and Geoffrey E. Hinton. Imagenet classification with deep convolutional neural networks. *Commun. ACM*, 60(6):84–90, 2017.
- [3] Tom Young, Devamanyu Hazarika, Soujanya Poria, and Erik Cambria. Recent trends in deep learning based natural language processing [review article]. *IEEE Comput. Intell. Mag.*, 13(3):55–75, 2018.
- [4] Ali Bou Nassif, Ismail Shahin, Imtinan Attili, Mohammad Azzeh, and Khaled Shaalan. Speech recognition using deep neural networks: A systematic review. *IEEE Access*, 7:19143–19165, 2019.
- [5] Anh Mai Nguyen, Jason Yosinski, and Jeff Clune. Deep neural networks are easily fooled: High confidence predictions for unrecognizable images. In *IEEE Conference on Computer Vision and Pattern Recognition, CVPR 2015, Boston, MA, USA, June 7-12, 2015*, pages 427–436. IEEE Computer Society, 2015.

- [6] Christian Szegedy, Wojciech Zaremba, Ilya Sutskever, Joan Bruna, Dumitru Erhan, Ian J. Goodfellow, and Rob Fergus. Intriguing properties of neural networks. In *2nd International Conference on Learning Representations, ICLR 2014, Banff, AB, Canada, April 14-16, 2014, Conference Track Proceedings*, 2014.
- [7] Dan Hendrycks and Kevin Gimpel. A baseline for detecting misclassified and out-of-distribution examples in neural networks. In *5th International Conference on Learning Representations, ICLR 2017, Toulon, France, April 24-26, 2017, Conference Track Proceedings*. OpenReview.net, 2017.
- [8] Matthias Hein, Maksym Andriushchenko, and Julian Bitterwolf. Why relu networks yield high-confidence predictions far away from the training data and how to mitigate the problem. In *IEEE Conference on Computer Vision and Pattern Recognition, CVPR 2019, Long Beach, CA, USA, June 16-20, 2019*, pages 41–50. Computer Vision Foundation / IEEE, 2019.
- [9] Marco Barreno, Blaine Nelson, Russell Sears, Anthony D. Joseph, and J. D. Tygar. Can machine learning be secure? In *Proceedings of the 2006 ACM Symposium on Information, Computer and Communications Security, ASIACCS 2006, Taipei, Taiwan, March 21-24, 2006*, pages 16–25. ACM, 2006.
- [10] Battista Biggio and Fabio Roli. Wild patterns: Ten years after the rise of adversarial machine learning. *Pattern Recognit.*, 84:317–331, 2018.
- [11] David M. J. Tax and Robert P. W. Duin. Growing a multi-class classifier with a reject option. *Pattern Recognit. Lett.*, 29(10):1565–1570, 2008.
- [12] Lihong Li, Michael L Littman, Thomas J Walsh, and Alexander L Strehl. Knows what it knows: a framework for self-aware learning. *Machine learning*, 82(3):399–443, 2011.
- [13] Ian J. Goodfellow, Jonathon Shlens, and Christian Szegedy. Explaining and harnessing adversarial examples. In *3rd International Conference on Learning Representations, ICLR 2015, San Diego, CA, USA, May 7-9, 2015, Conference Track Proceedings*, 2015.
- [14] Nicolas Papernot, Patrick D. McDaniel, Somesh Jha, Matt Fredrikson, Z. Berkay Celik, and Ananthram Swami. The limitations of deep learning in adversarial settings. In *IEEE European Symposium on Security and Privacy, EuroS&P 2016*, pages 372–387. IEEE, 2016.
- [15] Nicholas Carlini and David A. Wagner. Towards evaluating the robustness of neural networks. In *2017 IEEE Symposium on Security and Privacy, SP 2017, San Jose, CA, USA, May 22-26, 2017*, pages 39–57. IEEE Computer Society, 2017.
- [16] Aleksander Madry, Aleksandar Makelov, Ludwig Schmidt, Dimitris Tsipras, and Adrian Vladu. Towards deep learning models resistant to adversarial attacks. In *6th International Conference on Learning Representations, ICLR 2018, Vancouver, BC, Canada, April 30 - May 3, 2018, Conference Track Proceedings*. OpenReview.net, 2018.
- [17] Shiyu Liang, Yixuan Li, and R. Srikant. Enhancing the reliability of out-of-distribution image detection in neural networks. In *6th International Conference on Learning Representations, ICLR 2018, Vancouver, BC, Canada, April 30 - May 3, 2018, Conference Track Proceedings*. OpenReview.net, 2018.
- [18] Kimin Lee, Honglak Lee, Kibok Lee, and Jinwoo Shin. Training confidence-calibrated classifiers for detecting out-of-distribution samples. In *6th International Conference on Learning Representations, ICLR 2018, Vancouver, BC, Canada, April 30 - May 3, 2018, Conference Track Proceedings*. OpenReview.net, 2018.
- [19] Reuben Feinman, Ryan R. Curtin, Saurabh Shintre, and Andrew B. Gardner. Detecting adversarial samples from artifacts. *CoRR*, abs/1703.00410, 2017.
- [20] Weilin Xu, David Evans, and Yanjun Qi. Feature squeezing: Detecting adversarial examples in deep neural networks. In *25th Annual Network and Distributed System Security Symposium, NDSS 2018, San Diego, California, USA, February 18-21, 2018*. The Internet Society, 2018.
- [21] Xin Li and Fuxin Li. Adversarial examples detection in deep networks with convolutional filter statistics. In *IEEE International Conference on Computer Vision, ICCV 2017, Venice, Italy, October 22-29, 2017*, pages 5775–5783. IEEE Computer Society, 2017.
- [22] Kimin Lee, Kibok Lee, Honglak Lee, and Jinwoo Shin. A simple unified framework for detecting out-of-distribution samples and adversarial attacks. In *Advances in Neural Information*

- Processing Systems 31: Annual Conference on Neural Information Processing Systems 2018, NeurIPS 2018, 3-8 December 2018, Montréal, Canada*, pages 7167–7177, 2018.
- [23] Xingjun Ma, Bo Li, Yisen Wang, Sarah M. Erfani, Sudanthi N. R. Wijewickrema, Grant Schoenebeck, Dawn Song, Michael E. Houle, and James Bailey. Characterizing adversarial subspaces using local intrinsic dimensionality. In *6th International Conference on Learning Representations, ICLR 2018, Vancouver, BC, Canada, April 30 - May 3, 2018, Conference Track Proceedings*. OpenReview.net, 2018.
 - [24] Kevin Roth, Yannic Kilcher, and Thomas Hofmann. The odds are odd: A statistical test for detecting adversarial examples. In *Proceedings of the 36th International Conference on Machine Learning, ICML 2019, 9-15 June 2019, Long Beach, California, USA*, volume 97 of *Proceedings of Machine Learning Research*, pages 5498–5507. PMLR, 2019.
 - [25] Dongyu Meng and Hao Chen. MagNet: A two-pronged defense against adversarial examples. In *Proceedings of the 2017 ACM SIGSAC Conference on Computer and Communications Security, CCS 2017, Dallas, TX, USA, October 30 - November 03, 2017*, pages 135–147. ACM, 2017.
 - [26] Zhihao Zheng and Pengyu Hong. Robust detection of adversarial attacks by modeling the intrinsic properties of deep neural networks. In *Advances in Neural Information Processing Systems 31: Annual Conference on Neural Information Processing Systems 2018, NeurIPS 2018, 3-8 December 2018, Montréal, Canada*, pages 7924–7933, 2018.
 - [27] Nicolas Papernot and Patrick D. McDaniel. Deep k-nearest neighbors: Towards confident, interpretable and robust deep learning. *CoRR*, abs/1803.04765, 2018.
 - [28] David J. Miller, Yujia Wang, and George Kesidis. When not to classify: Anomaly detection of attacks (ADA) on DNN classifiers at test time. *Neural Computation*, 31(8):1624–1670, 2019.
 - [29] Puyudi Yang, Jianbo Chen, Cho-Jui Hsieh, Jane-Ling Wang, and Michael I. Jordan. ML-LOO: detecting adversarial examples with feature attribution. *CoRR*, abs/1906.03499, 2019.
 - [30] Nicholas Carlini and David A. Wagner. Adversarial examples are not easily detected: Bypassing ten detection methods. In *Proceedings of the 10th ACM Workshop on Artificial Intelligence and Security, AISec@CCS 2017, Dallas, TX, USA, November 3, 2017*, pages 3–14. ACM, 2017.
 - [31] Florian Tramèr, Nicholas Carlini, Wieland Brendel, and Aleksander Madry. On adaptive attacks to adversarial example defenses. *CoRR*, abs/2002.08347, 2020.
 - [32] Heinrich Jiang, Been Kim, Melody Y. Guan, and Maya R. Gupta. To trust or not to trust a classifier. In *Advances in Neural Information Processing Systems 31: Annual Conference on Neural Information Processing Systems 2018, NeurIPS 2018, 3-8 December 2018, Montréal, Canada*, pages 5546–5557, 2018.
 - [33] Chandramouli Shama Sastry and Sageev Oore. Detecting out-of-distribution examples with in-distribution examples and gram matrices. *CoRR*, abs/1912.12510, 2019.
 - [34] Battista Biggio, Blaine Nelson, and Pavel Laskov. Poisoning attacks against support vector machines. In *Proceedings of the 29th International Conference on Machine Learning, ICML 2012, Edinburgh, Scotland, UK, June 26 - July 1, 2012*. icml.cc / Omnipress, 2012.
 - [35] Luis Muñoz-González, Battista Biggio, Ambra Demontis, Andrea Paudice, Vasin Wongrasamee, Emil C. Lupu, and Fabio Roli. Towards poisoning of deep learning algorithms with back-gradient optimization. In *Proceedings of the 10th ACM Workshop on Artificial Intelligence and Security, AISec@CCS 2017, Dallas, TX, USA, November 3, 2017*, pages 27–38. ACM, 2017.
 - [36] Jacob Steinhardt, Pang Wei Koh, and Percy Liang. Certified defenses for data poisoning attacks. In *Advances in Neural Information Processing Systems 30: Annual Conference on Neural Information Processing Systems 2017, 4-9 December 2017, Long Beach, CA, USA*, pages 3517–3529, 2017.
 - [37] Seyed-Mohsen Moosavi-Dezfooli, Alhussein Fawzi, and Pascal Frossard. Deepfool: A simple and accurate method to fool deep neural networks. In *2016 IEEE Conference on Computer Vision and Pattern Recognition, CVPR 2016, Las Vegas, NV, USA, June 27-30, 2016*, pages 2574–2582. IEEE Computer Society, 2016.
 - [38] Alexey Kurakin, Ian J. Goodfellow, and Samy Bengio. Adversarial machine learning at scale. In *5th International Conference on Learning Representations, ICLR 2017, Toulon, France, April 24-26, 2017, Conference Track Proceedings*. OpenReview.net, 2017.

- [39] Seyed-Mohsen Moosavi-Dezfooli, Alhussein Fawzi, Omar Fawzi, and Pascal Frossard. Universal adversarial perturbations. In *2017 IEEE Conference on Computer Vision and Pattern Recognition, CVPR 2017, Honolulu, HI, USA, July 21-26, 2017*, pages 86–94. IEEE Computer Society, 2017.
- [40] Naveed Akhtar and Ajmal S. Mian. Threat of adversarial attacks on deep learning in computer vision: A survey. *IEEE Access*, 6:14410–14430, 2018.
- [41] Xiaoyong Yuan, Pan He, Qile Zhu, and Xiaolin Li. Adversarial examples: Attacks and defenses for deep learning. *IEEE Trans. Neural Networks Learn. Syst.*, 30(9):2805–2824, 2019.
- [42] Alhussein Fawzi, Seyed-Mohsen Moosavi-Dezfooli, and Pascal Frossard. Robustness of classifiers: from adversarial to random noise. In *Advances in Neural Information Processing Systems 29: Annual Conference on Neural Information Processing Systems 2016, December 5-10, 2016, Barcelona, Spain*, pages 1624–1632, 2016.
- [43] Alhussein Fawzi, Omar Fawzi, and Pascal Frossard. Analysis of classifiers’ robustness to adversarial perturbations. *Mach. Learn.*, 107(3):481–508, 2018.
- [44] David J Miller, Zhen Xiang, and George Kesidis. Adversarial learning targeting deep neural network classification: A comprehensive review of defenses against attacks. *Proceedings of the IEEE*, 108(3):402–433, 2020.
- [45] Varun Chandola, Arindam Banerjee, and Vipin Kumar. Anomaly detection: A survey. *ACM computing surveys (CSUR)*, 41(3):1–58, 2009.
- [46] Manqi Zhao and Venkatesh Saligrama. Anomaly detection with score functions based on nearest neighbor graphs. In *Advances in Neural Information Processing Systems 22: 23rd Annual Conference on Neural Information Processing Systems 2009. Proceedings of a meeting held 7-10 December 2009, Vancouver, British Columbia, Canada*, pages 2250–2258, 2009.
- [47] Saikiran Bulusu, Bhavya Kailkhura, Bo Li, Pramod K. Varshney, and Dawn Song. Anomalous instance detection in deep learning: A survey. *CoRR*, abs/2003.06979, 2020.
- [48] Jing Qian and Venkatesh Saligrama. New statistic in p-value estimation for anomaly detection. In *IEEE Statistical Signal Processing Workshop, SSP 2012, Ann Arbor, MI, USA, August 5-8, 2012*, pages 393–396. IEEE, 2012.
- [49] Larry Wasserman. *All of statistics: a concise course in statistical inference*. Springer Science & Business Media, 2013.
- [50] Bernard W Silverman. *Density estimation for statistics and data analysis*, volume 26. CRC press, 1986.
- [51] Sandrine Dudoit and Mark J Van Der Laan. *Multiple testing procedures with applications to genomics*. Springer Science & Business Media, 2007.
- [52] Ronald Aylmer Fisher. Statistical methods for research workers. In *Breakthroughs in statistics*, pages 66–70. Springer, 1992.
- [53] Daniel J Wilson. The harmonic mean p-value for combining dependent tests. *Proceedings of the National Academy of Sciences*, 116(4):1195–1200, 2019.
- [54] David Barber. *Bayesian reasoning and machine learning*. Cambridge University Press, 2012.
- [55] Timothy RC Read and Noel AC Cressie. *Goodness-of-fit statistics for discrete multivariate data*. Springer Science & Business Media, 2012.
- [56] Anish Athalye, Nicholas Carlini, and David A. Wagner. Obfuscated gradients give a false sense of security: Circumventing defenses to adversarial examples. In *Proceedings of the 35th International Conference on Machine Learning, ICML 2018, Stockholm, Sweden, July 10-15, 2018*, volume 80 of *Proceedings of Machine Learning Research*, pages 274–283. PMLR, 2018.
- [57] Chawin Sitawarin and David A. Wagner. Minimum-norm adversarial examples on KNN and KNN-based models. *CoRR*, abs/2003.06559, 2020.
- [58] Nicholas Frosst, Nicolas Papernot, and Geoffrey E. Hinton. Analyzing and improving representations with the soft nearest neighbor loss. In *Proceedings of the 36th International Conference on Machine Learning, ICML 2019, 9-15 June 2019, Long Beach, California, USA*, volume 97 of *Proceedings of Machine Learning Research*, pages 2012–2020. PMLR, 2019.

- [59] Alex Krizhevsky, Geoffrey Hinton, et al. Learning multiple layers of features from tiny images. 2009.
- [60] Yuval Netzer, Tao Wang, Adam Coates, Alessandro Bissacco, Bo Wu, and Andrew Y Ng. Reading digits in natural images with unsupervised feature learning. 2011.
- [61] Yann LeCun, Léon Bottou, Yoshua Bengio, and Patrick Haffner. Gradient-based learning applied to document recognition. *Proceedings of the IEEE*, 86(11):2278–2324, 1998.
- [62] Jonas Rauber, Wieland Brendel, and Matthias Bethge. Foolbox: A python toolbox to benchmark the robustness of machine learning models. In *Reliable Machine Learning in the Wild Workshop, 34th International Conference on Machine Learning*, 2017.
- [63] Jesse Davis and Mark Goadrich. The relationship between Precision-Recall and ROC curves. In *Proceedings of the 23rd international conference on Machine learning*, pages 233–240, 2006.
- [64] Peter Flach and Meelis Kull. Precision-recall-gain curves: PR analysis done right. In *Advances in neural information processing systems*, pages 838–846, 2015.
- [65] Tom Fawcett. An introduction to ROC analysis. *Pattern recognition letters*, 27(8):861–874, 2006.
- [66] Steven M Kay. Fundamentals of statistical signal processing. Detection theory, volume ii. *Printice Hall PTR*, pages 1545–5971, 1998.
- [67] Kevin M Carter, Raviv Raich, and Alfred O Hero III. On local intrinsic dimension estimation and its applications. *IEEE Transactions on Signal Processing*, 58(2):650–663, 2009.
- [68] Alessio Ansuini, Alessandro Laio, Jakob H Macke, and Davide Zoccolan. Intrinsic dimension of data representations in deep neural networks. *arXiv preprint arXiv:1905.12784*, 2019.
- [69] Laurent Amsaleg, Oussama Chelly, Teddy Furon, Stéphane Girard, Michael E Houle, Ken-ichi Kawarabayashi, and Michael Nett. Estimating local intrinsic dimensionality. In *Proceedings of the 21th ACM SIGKDD International Conference on Knowledge Discovery and Data Mining*, pages 29–38. ACM, 2015.
- [70] Alex Krizhevsky, Ilya Sutskever, and Geoffrey E Hinton. Imagenet classification with deep convolutional neural networks. In *Advances in neural information processing systems*, pages 1097–1105, 2012.
- [71] Kaiming He, Xiangyu Zhang, Shaoqing Ren, and Jian Sun. Deep residual learning for image recognition. In *Proceedings of the IEEE conference on computer vision and pattern recognition*, pages 770–778, 2016.
- [72] Yaroslav Bulatov. NotMNIST dataset. <http://yaroslavvb.com/upload/notMNIST/>, 2011.
- [73] Fabian Pedregosa, Gaël Varoquaux, Alexandre Gramfort, Vincent Michel, Bertrand Thirion, Olivier Grisel, Mathieu Blondel, Peter Prettenhofer, Ron Weiss, Vincent Dubourg, et al. Scikit-learn: Machine learning in python. *Journal of machine learning research*, 12(Oct):2825–2830, 2011.
- [74] Adam Paszke, Sam Gross, Soumith Chintala, Gregory Chanan, Edward Yang, Zachary DeVito, Zeming Lin, Alban Desmaison, Luca Antiga, and Adam Lerer. Automatic differentiation in PyTorch. 2017.
- [75] Wei Dong, Charikar Moses, and Kai Li. Efficient k-nearest neighbor graph construction for generic similarity measures. In *Proceedings of the 20th international conference on World wide web*, pages 577–586, 2011.
- [76] Xiaofei He, Deng Cai, Shuicheng Yan, and Hong-Jiang Zhang. Neighborhood preserving embedding. In *Tenth IEEE International Conference on Computer Vision (ICCV’05) Volume 1*, volume 2, pages 1208–1213. IEEE, 2005.
- [77] Sebastian Ruder. An overview of gradient descent optimization algorithms. *CoRR*, abs/1609.04747, 2016.

Appendix

A Harmonic Mean p-value Method

The harmonic mean p-value (HMP) [53] is a recently proposed method for combining p-values from a large number of dependent tests. It is rooted in ideas from Bayesian model averaging and has some desirable properties such as robustness to positive dependency between the p-values, and an ability to detect small statistically significant groups from a large number of p-values (tests). In our problem, the inverse of the weighted harmonic mean of the p-values from multiple layers and layer pairs, conditioned on the predicted class and on each candidate true class, are given respectively by

$$\begin{aligned} q_{\text{hmp}}(\mathbf{t}_p | \hat{c})^{-1} &= \sum_{l=0}^L w_l q(t_p^{(l)} | \hat{c})^{-1} + \sum_{\substack{l_1, l_2 \in [L]^2 \\ l_2 > l_1}} w_{l_1, l_2} q(t_p^{(l_1)}, t_p^{(l_2)} | \hat{c})^{-1} \\ q_{\text{hmp}}(\mathbf{t}_s | c)^{-1} &= \sum_{l=0}^L w_l q(t_s^{(l)} | c)^{-1} + \sum_{\substack{l_1, l_2 \in [L]^2 \\ l_2 > l_1}} w_{l_1, l_2} q(t_s^{(l_1)}, t_s^{(l_2)} | c)^{-1}, \quad \forall c \in [m]. \end{aligned} \quad (15)$$

The weights w_l and w_{l_1, l_2} should be non-negative such that they sum to 1; they can be used to incorporate any prior knowledge about the relative importance of different layers and layer pairs. In practice, we set all the weights to be equal.

In our experiments, we found the HMP method to have comparable or slightly worse performance compared to the Fisher’s method of combining p-values (§ 3.2). This is surprising given the simplistic assumption of independent tests made by Fisher’s method. We conjecture that Fisher’s method achieves better detection at the expense of a higher FPR, while the HMP method has a more conservative detection rate with a lower FPR. To maintain clarity in the experiments, we only report results based on Fisher’s method.

B Test Statistics at the DNN Layers

In section § 3.7, we presented the multinomial test statistic which is based on class counts from the k -nearest neighbors of a DNN layer representation. To demonstrate the generality of the proposed method, we present and evaluate three additional test statistics that are also based on local statistical properties calculated from the k -nearest neighbors of a DNN layer representation. For this discussion, we define the following additional terms. Let

$$\mathcal{X}_c^{(l)} = \{\mathbf{x}_n^{(l)}, n \in [N] : c_n = c\}, \quad c \in [m]$$

define the set of representations from layer l corresponding to samples labeled into class c . Similarly, let

$$\tilde{\mathcal{X}}_c^{(l)} = \{\mathbf{x}_n^{(l)}, n \in [N] : \hat{c}_n = c\}, \quad c \in [m]$$

define the set of representations from layer l corresponding to the samples predicted into class c .

Binomial class count based test statistic

This is a specialization of the multinomial test statistic, wherein instead of focusing on the kNN counts from all classes, we focus on the kNN count from a particular class (either the predicted class or a candidate true class). Consider an input \mathbf{x} with layer representations $\mathbf{x}^{(l)}$, $l = 0, 1, \dots, L$ and predicted class \hat{c} . Let $k_{\hat{c}}^{(l)} \in \{0, 1, \dots, k\}$ be the number of k -nearest neighbors from class \hat{c} for the representation $\mathbf{x}^{(l)}$ from layer l . This count can be interpreted as the number of successes $k_{\hat{c}}^{(l)}$ in a Binomial distribution with k trials. We define the binomial test statistic given a class c as the proportion of k -nearest neighbors that are not from the same class c . The test statistics at layer l conditioned on the predicted class \hat{c} and on each candidate true class are defined respectively as,

$$\begin{aligned} T_p(\mathbf{x}^{(l)}, \hat{c}) &= \frac{k - k_{\hat{c}}^{(l)}}{k}, \\ T_s(\mathbf{x}^{(l)}, c) &= \frac{k - k_c^{(l)}}{k}, \quad \forall c \in [m]. \end{aligned} \quad (16)$$

The test statistics are bounded to $[0, 1]$ and measure the non-conformity of the class labels among the k-nearest neighbors of a layer representation, with larger values corresponding to a larger non-conformity. We note the similarity of this test statistic with the non-conformity score computed by the deep KNN method [27], with a key difference that deep KNN calculates a single non-conformity score (per class) by summing the non-conforming class counts across the layers.

Trust Score based test statistic

The trust score was proposed by Jiang *et al.* [32] as a confidence score for a classifier that indicates when the classifier’s prediction on a test input is likely to be correct. We first provide an informal definition of the α -high density set $H_\alpha(f)$ for $\alpha \in [0, 1]$ and a continuous density function f as – the set of all points with density larger than a certain value λ_α such that $1 - \alpha$ fraction of the probability mass is contained in $H_\alpha(f)$ (refer to Jiang *et al.* [32] for the formal definition). Given a set of points \mathcal{X}_c from each class $c \in [m]$, the trust score estimates the α -high density set $\hat{H}_\alpha(f_c)$ for each class-conditional density f_c , $c \in [m]$ using the kNN distances of points from \mathcal{X}_c . For the special case of $\alpha = 0$ the density level-set estimate reduces to the set of all points from class c , i.e., $\hat{H}_0(f_c) = \mathcal{X}_c$.

Given a test input \mathbf{x} that is predicted into class \hat{c} by the classifier, the trust score associated with the classifier’s prediction on \mathbf{x} is defined as [32]

$$\xi(\mathbf{x}, \hat{c}) = \frac{\min_{i \in [m] \setminus \{\hat{c}\}} d_{\text{haus}}(\mathbf{x}, \hat{H}_\alpha(f_i))}{d_{\text{haus}}(\mathbf{x}, \hat{H}_\alpha(f_{\hat{c}}))},$$

where d_{haus} is the Hausdorff distance, which in this case reduces to the nearest neighbor distance $d_{\text{haus}}(\mathbf{x}, \mathcal{X}) = \min_{\mathbf{y} \in \mathcal{X}} d(\mathbf{x}, \mathbf{y})$ between a point \mathbf{x} and a set \mathcal{X} . In other words, the trust score is the ratio of the minimum distance from a point to the α -high density set of a class different from the predicted class, to the distance from a point to the α -high density set of the predicted class. The score is non-negative and unbounded above, with larger values indicating a higher level of trust or confidence in the classifier’s prediction.

For an input \mathbf{x} with representation $\mathbf{x}^{(l)}$ at layer l and predicted class \hat{c} , we define the test statistic conditioned on the predicted class as the inverse of the trust score

$$T_p(\mathbf{x}^{(l)}, \hat{c}) = \frac{d_{\text{haus}}(\mathbf{x}^{(l)}, \tilde{\mathcal{X}}_{\hat{c}}^{(l)})}{\min_{i \in [m] \setminus \{\hat{c}\}} d_{\text{haus}}(\mathbf{x}^{(l)}, \tilde{\mathcal{X}}_i^{(l)})} \quad (17)$$

so that an anomalous inputs (with a low trust score) will have a large values for this test statistic. Note that we use the special case of the trust score with $\alpha = 0$ for simplicity. The set $\tilde{\mathcal{X}}_{\hat{c}}^{(l)}$ is a representative sample of layer representations from the class-conditional density given the predicted class $\hat{C} = \hat{c}$. Similarly, the test statistics at layer l conditioned on each candidate true class are defined as

$$T_s(\mathbf{x}^{(l)}, c) = \frac{d_{\text{haus}}(\mathbf{x}^{(l)}, \mathcal{X}_c^{(l)})}{\min_{i \in [m] \setminus \{c\}} d_{\text{haus}}(\mathbf{x}^{(l)}, \mathcal{X}_i^{(l)})}, \quad \forall c \in [m]. \quad (18)$$

In this case, the set $\mathcal{X}_c^{(l)}$ is a representative sample of layer representations from the class-conditional density given the true class $C = c$.

Local Intrinsic Dimensionality based test statistic

Local intrinsic dimensionality (LID) at a point provides an indication of the dimension of the sub-manifold containing the point that would best fit the distribution of data in a local neighborhood of that point [67, 68]. For a formal definition of LID in terms of the cumulative distribution function of the distance from a point to other points from the same distribution, the reader is referred to prior works [23, 69]. In practice, LID is estimated from the distances of a point to its k-nearest neighbors using ideas from extreme value theory. We use the maximum likelihood estimator (MLE) of LID from Amsaleg *et al.* [69] that is also used in the work of Ma *et al.* [23] to estimate the LID of DNN layer representations. Consider a point \mathbf{x} whose distances to its k-nearest neighbors from a set of points \mathcal{X} are denoted by $r_i(\mathbf{x}, \mathcal{X})$, $i = 1, \dots, k$. The MLE estimate of LID from Amsaleg *et al.* [69] is given by

$$\widehat{\text{LID}}(\mathbf{x}, \mathcal{X}) = - \left(\frac{1}{k} \sum_{i=1}^k \log \frac{r_i(\mathbf{x}, \mathcal{X})}{r_k(\mathbf{x}, \mathcal{X})} \right)^{-1}.$$

For an input \mathbf{x} with representation $\mathbf{x}^{(l)}$ at layer l and predicted class \hat{c} , we define the test statistics based on LID conditioned on the predicted class \hat{c} and on each candidate true class as

$$\begin{aligned} T_p(\mathbf{x}^{(l)}, \hat{c}) &= \widehat{\text{LID}}(\mathbf{x}^{(l)}, \mathcal{X}_{\hat{c}}^{(l)}), \\ T_s(\mathbf{x}^{(l)}, c) &= \widehat{\text{LID}}(\mathbf{x}^{(l)}, \mathcal{X}_c^{(l)}), \quad \forall c \in [m]. \end{aligned} \quad (19)$$

We expect anomalous inputs to the DNN to produce test statistics (LID values) that are larger than that observed on natural inputs, as observed by Ma *et al.* [23] on adversarial inputs.

Combining Multiple Test Statistics.

We note that it is straightforward to include more than one test statistic per-layer in the framework of ReBeL. For example, the multinomial, binomial, and trust score based test statistics could be calculated at each layer, resulting in a test statistic vector of length $3(L + 1)$. With this change, the method for estimating p-values from the test statistics, either combined or multivariate, and the scoring function for adversarial and OOD detection do not require any modifications. Combining multiple test statistics in this way could be an approach to improving the detection performance of ReBeL, with some increase in the computation. It may also be argued that it is harder for a defense-aware adaptive attacker to generate adversarial samples that can evade a detector based on multiple test statistics at the DNN layers.

In Appendix E.5, we provide results comparing the performance of ReBeL with the test statistics defined here on the adversarial detection task.

C Details and Extensions of the Custom Attack

C.1 Setting the Kernel Scale

The scale of the Gaussian kernel for a given clean input \mathbf{x} and for each layer σ_l determines the effective number of samples that contribute to the soft count approximating the k-NN counts in Eq. (14). Intuitively, we want the kernel to have a value close to 1 for points within a distance of η_l (the k-NN radius centered on $\mathbf{f}_l(\mathbf{x})$), and decay rapidly to 0 for larger distances. Suppose $\mathcal{N}_k(\mathbf{f}_l(\mathbf{x}))$ is the index set of the k nearest neighbors of $\mathbf{f}_l(\mathbf{x})$ from the l -th layer representations, then the probability of selecting the k nearest neighbors is given by

$$h_1(\sigma_l) = \frac{\sum_{n \in \mathcal{N}_k(\mathbf{f}_l(\mathbf{x}))} e^{-\frac{1}{\sigma_l^2} d(\mathbf{f}_l(\mathbf{x}), \mathbf{f}_l(\mathbf{x}_n))^2}}{\sum_{n=1}^N e^{-\frac{1}{\sigma_l^2} d(\mathbf{f}_l(\mathbf{x}), \mathbf{f}_l(\mathbf{x}_n))^2}}.$$

We could choose σ_l to maximize this probability and push it close to 1. However, this is likely to result in a very small value for σ_l , which would concentrate all the probability mass on the nearest neighbor. To ensure that the probability mass is distributed sufficiently uniformly over the k nearest neighbors we add the following normalized entropy term as a regularizer

$$h_2(\sigma_l) = \frac{1}{\log k} \sum_{i \in \mathcal{N}_k(\mathbf{f}_l(\mathbf{x}))} q_i(\sigma_l) \log \frac{1}{q_i(\sigma_l)},$$

where

$$q_i(\sigma_l) = \frac{e^{-\frac{1}{\sigma_l^2} d(\mathbf{f}_l(\mathbf{x}), \mathbf{f}_l(\mathbf{x}_i))^2}}{\sum_{j \in \mathcal{N}_k(\mathbf{f}_l(\mathbf{x}))} e^{-\frac{1}{\sigma_l^2} d(\mathbf{f}_l(\mathbf{x}), \mathbf{f}_l(\mathbf{x}_j))^2}}.$$

Both terms $h_1(\sigma_l)$ and $h_2(\sigma_l)$ are bounded to the interval $[0, 1]$. We set a suitable σ_l by maximizing a convex combination of the two terms, *i.e.*,

$$\max_{\sigma_l \in \mathbb{R}_+} (1 - \alpha) h_1(\sigma_l) + \alpha h_2(\sigma_l). \quad (20)$$

We set α to 0.5 in experiments and use a simple line search to find the approximate maximizer of Eq. (20).

C.2 Untargeted Attack

The formulation in § 4, where a specific class $c' \neq c$ is chosen, is used to create a targeted attack. Alternatively, a simple modification to Eq. (13) that considers the log-odds $\log \frac{p_c}{1-p_c}$ of class c can be used to create an untargeted attack, resulting in the following objective function to be minimized:

$$J(\zeta) = \|\zeta\|_2^2 + \lambda \log \sum_{l=0}^L \sum_{\substack{n=1:N \\ c_n=c}} r(\mathbf{f}_l(\mathbf{x} + \zeta), \mathbf{f}_l(\mathbf{x}_n), \sigma_l^2) - \lambda \log \sum_{l=0}^L \sum_{\substack{n=1:N \\ c_n \neq c}} r(\mathbf{f}_l(\mathbf{x} + \zeta), \mathbf{f}_l(\mathbf{x}_n), \sigma_l^2)$$

C.3 Alternate Loss Function

Starting from equation Eq. (13), but now assuming that the probability estimate for a particular class c (based on the k-NN model) factors into a product of probabilities across the layers of the DNN (*i.e.*, independence assumption), we get

$$\log \frac{p_c}{p_{c'}} = \log \frac{k_c}{k_{c'}} = \log \frac{\prod_l k_c^{(l)} / k}{\prod_l k_{c'}^{(l)} / k} = \sum_{l=0}^L \log k_c^{(l)} - \sum_{l=0}^L \log k_{c'}^{(l)}.$$

Using the soft count approximation based on the Gaussian kernel (as before) leads to the following alternative loss function for the targeted custom attack

$$J(\zeta) = \|\zeta\|_2^2 + \lambda \sum_{l=0}^L \log \sum_{\substack{n=1:N \\ c_n=c}} r(\mathbf{f}_l(\mathbf{x} + \zeta), \mathbf{f}_l(\mathbf{x}_n), \sigma_l^2) - \lambda \sum_{l=0}^L \log \sum_{\substack{n=1:N \\ c_n=c'}} r(\mathbf{f}_l(\mathbf{x} + \zeta), \mathbf{f}_l(\mathbf{x}_n), \sigma_l^2)$$

In contrast to Eq. (14), this loss function considers the class probability estimates from each layer instead of a single class probability estimate based on the cumulative kNN counts across the layers. A similar modification can be applied for the untargeted attack as well.

D Additional Implementation Details

D.1 Computing Platform

Our experiments were performed on a single server running Ubuntu 18.04 with 128 GB memory, 4 NVIDIA GeForce RTX 2080 GPUs, and 32 CPU cores.

D.2 Datasets & DNN Architectures

A summary of the image classification datasets we used, the architecture and test set performance of the corresponding DNNs are given in Table 3. Each dataset has 10 image classes. We followed recommended best practices used for training DNNs on image classification problems. We did not train a DNN on the Not-MNIST dataset because this dataset is used only for evaluation in the out-of-distribution detection experiments.

| Dataset | Input dimension | Train size | Test size | Test Accuracy | Architecture |
|----------------|-------------------------|------------|-----------|---------------|-----------------------|
| MNIST [61] | $28 \times 28 \times 1$ | 50,000 | 10,000 | 99.12 | AlexNet [70] |
| SVHN [60] | $32 \times 32 \times 3$ | 73,257 | 26,032 | 89.42 | 2 Conv. + 3 FC layers |
| CIFAR-10 [59] | $32 \times 32 \times 3$ | 50,000 | 10,000 | 95.45 | ResNet-34 [71] |
| Not-MNIST [72] | $28 \times 28 \times 1$ | 500,000 | 18,724 | N/A | N/A |

Table 3: Datasets & DNN Architectures.

D.3 OOD Detection Experiment Setup

We evaluated OOD detection using the following dataset pairs: 1) MNIST images as in-distribution and Not-MNIST [72] images as out-distribution (outlier), 2) CIFAR-10 images as in-distribution and SVHN images as out-distribution. As before, we used stratified 5-fold cross-validation and calculated the average performance metrics from the test folds. We compared the performance of ReBeL with Mahalanobis, DKNN, and Trust; Odds and LID are excluded from this experiment because they mainly focus on adversarial detection. For ReBeL, we used Eq. (5) with p-values calculated using both Fisher’s method and the aK-LPE method. Since Mahalanobis is a supervised method, it uses both in-distribution and out-distribution data from the training folds, while the remaining methods (all unsupervised) use only the in-distribution data from the training folds. To promote fairness in the comparison, we excluded out-distribution data from one half of the classes from the training folds, and included out-distribution data from *only* the excluded classes in the test folds. Additionally, in the test folds we included image samples with pixel values randomly generated from a uniform distribution with the same range as the valid images. The number of random samples is set equal to the number of test fold samples from a single class.

D.4 Method Implementations

The code associated with our work can be accessed [here](#)¹³. We utilized the authors original implementation for the following methods: (i) deep mahalanobis detector¹⁴, (ii) the odds are odd detector¹⁵. We implemented the remaining detection methods, viz. LID, DKNN, and Trust, and this is available as part of our released code. All implementations are in Python3 and are based on standard scientific computing libraries such as Numpy, Scipy, and Scikit-learn [73]. We used PyTorch as the deep learning and automatic differentiation backend [74]. We perform approximate nearest neighbor search using the NNDescent method [75] to efficiently construct and query from kNN graphs at the DNN layer representations. We used the implementation of NNDescent based on the library PyNNDescent¹⁶. Our implementation of ReBeL is highly modular, allowing for new test statistics to be easily plugged in to the existing implementation. We provide implementations of the following test statistics: (i) multinomial class counts, (ii) binomial class counts, (iii) trust score, (iv) local intrinsic dimensionality, and (v) average kNN distance.

In our experiments with ReBeL, where Fisher’s method or HMP method are used for combining the p-values, we included p-values estimated from the individual layers (listed in Tables 4, 5, and 6) and from all distinct layer pairs. The number of nearest neighbors k is set to be a function of the number of samples n using the heuristic $k = \lceil n^{0.4} \rceil$. For methods like DKNN, LID, and Trust that use k , we found that setting k in this way produced comparable results to that obtained over a range of k values. Therefore, to maintain consistency, we set k for all the (applicable) methods using the choice $k = \lceil n^{0.4} \rceil$.

For the method Trust, we applied the trust score to the input, logit (pre-softmax) layer, and the fully-connected layer prior to the logit (pre-logit) layer. Since it was reported in Jiang *et al.* [32] that the trust score works well mainly in low-dimensional settings, we applied the same dimensionality reduction that was applied to ReBeL (see Tables 4, 5, and 6) on the input and pre-logit layer representations. We found the pre-logit layer to produce the best detection performance in our experiments. Hence, we report results for Trust with the pre-logit layer in all our experiments. The constant α , which determines the fraction of samples with lowest empirical density to be excluded from the density level sets, is set to 0 in our experiments. We explored a few other values of α , but did not find a significant difference in performance. This is consistent with the observation in Section 5.3 of [32].

The methods Mahalanobis and LID train a logistic classifier to discriminate adversarial samples from natural samples. The regularization constant of the logistic classifier is found by searching (over a set of 10 logarithmically spaced values between 0.0001 to 10000) for the value that leads to the largest average test-fold area under the ROC curve, in a 5-fold stratified cross-validation setup.

For the method Odds, the implementation of the authors returns a binary (0 / 1) detection decision instead of a continuous score that can be used to rank adversarial samples. The binary decision

¹³<https://github.com/jayaram-r/adversarial-detection>

¹⁴https://github.com/pokaxpoka/deep_Mahalanobis_detector

¹⁵https://github.com/yk/icml19_public

¹⁶<https://github.com/lmcinnes/pyndescent>

is based on applying z-score normalization to the original score, and comparing it to the 99.9-th percentile of the standard Gaussian density. Instead of using the thresholded decision, we used the z-score-normalized score of Odds in order to get a continuous score that is required by the metrics average precision and pAUC- α .

Details on the DNN Layer Representations

The DNN layers used in our experiments and their raw dimensionality are listed for the three datasets in Tables 4, 5, and 6. An exception to this is the LID method, for which we follow the implementation of Ma *et al.* [23] and calculate the LID features from all the intermediate layers. For DKNN and LID, we did not apply any dimensionality reduction or pre-processing of the layer representations to be consistent with the respective papers. For Mahalanobis, the implementation of the authors performs global average pooling at each convolutional layer to transform a $C \times W \times H$ tensor (with C channels) to a C -dimensional vector.

For ReBeL, we use the neighborhood preserving projection (NPP) method [76] to perform dimensionality reduction on the layer representations. We chose NPP because it performs an efficient linear projection that attempts to preserve the neighborhood structure in the original space as closely as possible in the projected (lower dimensional) space. Working with the lower dimensional layer representations mitigates problems associated with the curse of dimensionality, and significantly reduces the memory utilization and the running time of ReBeL. The original dimension, intrinsic dimension estimate, and the projected dimension of the layer representations for the three datasets are listed in Tables 4, 5, and 6. We did not apply dimension reduction to the logit layer because it has only 10 dimensions.

| Layer | Layer index | Original dimension | Intrinsic dimension estimate | Projected dimension |
|----------------------------|-------------|--------------------|------------------------------|---------------------|
| Input | 0 | 784 | 13 | 31 |
| Conv-1 + ReLu | 1 | 21632 | 22 | 53 |
| Conv-2 + Maxpool + Dropout | 2 | 9216 | 18 | 77 |
| FC-1 + ReLu + Dropout | 3 | 128 | 9 | 90 |
| FC-2 (Logit) | 4 | 10 | 6 | 10 |

Table 4: Layer representations of the DNN trained on MNIST. The output of the block listed in the first column is used as the layer representation.

| Layer | Layer index | Original dimension | Intrinsic dimension estimate | Projected dimension |
|-----------------------------------|-------------|--------------------|------------------------------|---------------------|
| Input | 0 | 3072 | 18 | 43 |
| Conv-1 + ReLu | 1 | 57600 | 38 | 380 |
| Conv-2 + ReLu + Maxpool + Dropout | 2 | 12544 | 42 | 400 |
| FC-1 + ReLu + Dropout | 3 | 512 | 12 | 120 |
| FC-2 + ReLu + Dropout | 4 | 128 | 7 | 10 |
| FC-3 (Logit) | 5 | 10 | 4 | 10 |

Table 5: Layer representations of the DNN trained on SVHN. The output of the block listed in the first column is used as the layer representation.

The procedure we used for determining the projected dimension is summarized as follows. We used the training partition of each dataset (that was used to train the DNN) for this task in order to avoid introducing any bias on the test partition (which is used for the detection and corrected classification experiments). At each layer, we first estimate the intrinsic dimension (ID) as the median of the LID estimates of the samples, found using the method of Amsaleg *et al.* [69]. The ID estimate d_{int} is used as a lower bound for the projected dimension. Using a 5-fold stratified cross-validation setup, we search over 20 linearly spaced values in the interval $[d_{\text{int}}, 10 d_{\text{int}}]$ for the projected dimension (found using NPP) that results in the smallest average test-fold error rate for a standard k-nearest neighbors classifier. The resulting projected dimensions are given in Tables 4, 5, and 6.

| Layer | Layer index | Original dimension | Intrinsic dimension estimate | Projected dimension |
|---------------------------|-------------|--------------------|------------------------------|---------------------|
| Input | 0 | 3072 | 25 | 48 |
| Conv-1 + BatchNorm + ReLU | 1 | 65536 | 33 | 330 |
| Residual block-1 | 2 | 65536 | 58 | 580 |
| Residual block-2 | 3 | 32768 | 59 | 590 |
| Residual block-3 | 4 | 16384 | 28 | 28 |
| Residual block-4 | 5 | 8192 | 15 | 15 |
| 2D Avg. Pooling | 6 | 512 | 9 | 9 |
| FC (Logit) | 7 | 10 | 8 | 10 |

Table 6: Layer representations of the ResNet-34 trained on CIFAR-10. The output of the block listed in the first column is used as the layer representation.

Note on Performance Calculation

The following procedure is used to calculate performance metrics as a function of the perturbation norm of adversarial samples. Suppose there are N_a adversarial samples and N_n natural samples in a test set, with $N = N_a + N_n$. Define the maximum proportion of adversarial samples $p_a = N_a / N$. The adversarial samples are first sorted in increasing order of their perturbation norm. The proportion of adversarial samples is varied over 12 equally-spaced values between 0.005 and $\min(0.3, p_a)$. For a given proportion p_i , the top $N_i = \lceil p_i N \rceil$ adversarial samples (sorted by norm) are selected. The perturbation norm of all these adversarial samples will be below a certain value; this value is shown on the x-axis of the performance plots. The performance metrics (average precision, pAUC- α etc.) are then calculated from the N_i adversarial samples and the N_n natural samples.

In order to calculate the performance metrics as a function of the proportion of adversarial or OOD (anomalous) samples, the only difference is that we do not sort the anomalous samples in a deterministic way. For a given proportion p_i , we select $N_i = \lceil p_i N \rceil$ anomalous samples at random uniformly, and calculate the performance metrics based on the N_i anomalous and N_n natural samples. To account for variability, this is repeated over 100 random subsets of N_i anomalous samples each, and the median value of the performance metrics is reported. Note that the detection methods need to score the samples only once, and the above calculations can be done based on the saved scores.

D.5 Details on the Adversarial Attacks

We list below the parameters of the adversarial attack methods we implemented using Foolbox [62]. We utilize the same variable names used by Foolbox in order to enable easy replication.

- FGSM: `max_epsilon=1, p_norm = inf`
- PGD: `epsilon = [1/255, 3/255, ..., 21/255]` `stepsize = 0.05`, `binary_search = False`, `iterations = 40, p_norm = inf`
- CW: `confidence = [0, 6, 14, 22]`, `max_iterations = 750, p_norm = 2`

For the adversarial detection experiments in § 5.1, we reported results for the attack parameter setting that would produce adversarial samples with the least perturbation norm in order to make the detection task challenging. This corresponds to `epsilon = 1 / 255` for the PGD attack, `confidence = 0` for the CW attack, and `max_epsilon = 1` for the FGSM attack (the only parameter value used). The adversarial data are generated once from the clean data corresponding to each training fold and test fold, and saved to files for reuse in the experiments. This way there is no randomness arising from the adversarial samples.

Custom Attack:

Here we provide additional details on the custom attack method proposed in § 4. The constant λ in the objective function controls the perturbation norm of the adversarial sample, and smaller values of λ lead to solutions with a smaller perturbation norm. We follow the approach of Carlini *et al.* [15] to set λ to the smallest possible value that leads to a successful adversarial perturbation. This is found using a bisection line search over ten steps. An adversarial input is considered successful if it

modifies the initially-correct class prediction of the defense method (given by Eq. (7) for ReBeL). We also follow the approach of Carlini *et al.* [15] to implicitly constraint the adversarial inputs to lie in the same range as the original inputs using the hyperbolic tangent and its inverse function. Suppose the inputs lie in the range $[a, b]^d$, the following sequence of transformations is applied to each component of the vectors

$$\begin{aligned} z_i &= \tanh^{-1}\left(2 \frac{x_i - a}{b - a} - 1\right) \\ z'_i &= z_i + w_i \\ x'_i &= (b - a) \frac{1}{2} (1 + \tanh(z_i + w_i)) + a \end{aligned}$$

effectively allowing the perturbation \mathbf{w} to be optimized over \mathbb{R}^d . The resulting unconstrained optimization is then solved using RMSProp for tuning gradient descent with adaptive learning rate [77]. We set the maximum number of gradient descent steps to 1000. In our experiments throughout the paper, the custom attack targets the variant of ReBeL based on Fisher’s method and the multinomial test statistic.

E Additional Experiments

E.1 Results on the FGSM Attack

Figure 5 presents the average precision of the different detection methods as a function of the l_2 norm of perturbation for the FGSM attack method. It is clear that both variants of ReBeL outperform the other methods, consistent with the trend observed on other attacks in § 5.

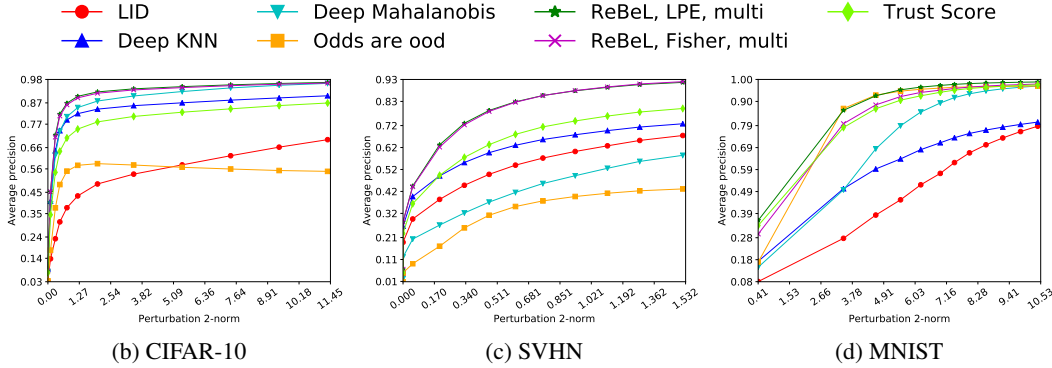


Figure 5: Average precision on the FGSM attack for all datasets.

E.2 Evaluation of Partial Area Under the ROC Curve

Here we compare the performance of methods using pAUC-0.2, a metric calculating the partial area under the ROC curve for FPR below 0.2. Comparing the area under the entire ROC curve can lead to misleading interpretations because it includes FPR values that one would rarely choose to operate in. Therefore, to reflect realistic operating conditions, we chose a maximum FPR of 0.2. Recall that for the PGD attack we vary the proportion of adversarial samples along the x-axis because most of the samples from this attack have the same perturbation norm.

On the CIFAR-10 dataset (Figure 6), we observe that ReBeL has better performance than the other methods in most cases. On the custom attack, Mahalanobis has slightly better performance than ReBeL with the multivariate p-value estimation method (aK-LPE). We make similar observations on the SVHN dataset (Figure 7), with a minor exception on the custom attack where the Odds method performs better than ReBeL as the perturbation norm increases.

On the MNIST dataset (Figure 8), we observe some different trends in the performance. On the CW and FGSM attacks, the methods Odds and Trust perform comparably or slightly better than ReBeL (particularly the variant based on Fisher’s method). On the custom attack, the performance of

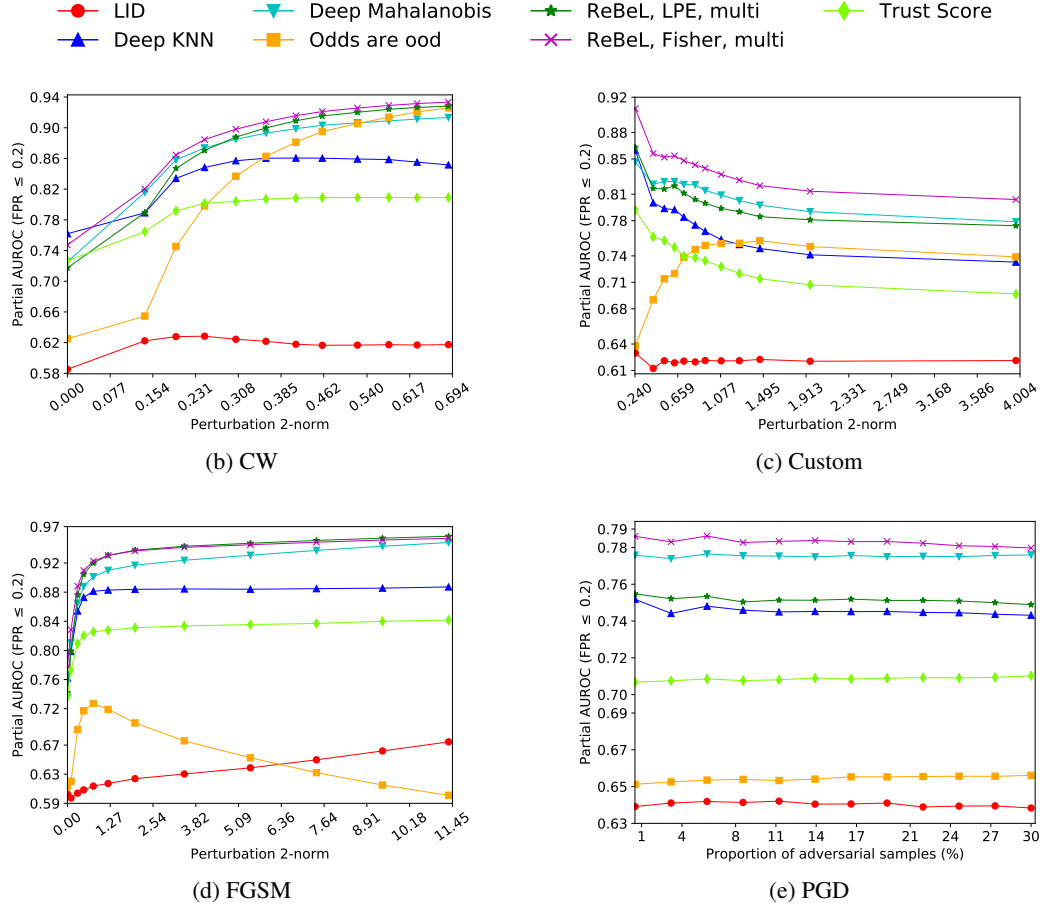


Figure 6: CIFAR-10 experiments: pAUC-0.2 for different attacks.

ReBeL based on Fisher’s method decreases significantly as the perturbation norm increases. On the other hand, the variant of ReBeL based of the aK-LPE method outperforms the other methods on this attack. We think that this contrast in performance is due to the fact that the custom attack samples were optimized to fool the variant of ReBeL based on Fisher’s method. Also, attack samples with higher perturbation norm are more likely to be successful. On the PGD attack, Odds outperforms the other methods, but the pAUC-0.2 of all methods, except LID and DKNN, are higher than 0.95 in this case. We conjecture that the good performance of most methods on MNIST could be due to the simplicity of the space of image inputs and the classification problem.

E.3 Results on the MNIST Dataset

In Figure 9, we compare the average precision of different methods on the MNIST dataset for the CW, PGD, and custom attacks (results for the FGSM attack were presented in § E.1). We observe that Odds has good performance on this dataset, outperforming ReBeL in some cases. The method Trust (which uses the pre-logit, fully connected layer) also performs well on this dataset. This could be due to the fact that on the MNIST dataset, the attack samples exhibit very distinctive patterns at the logit and pre-logit DNN layers, which are the focus of the methods Odds and Trust. We note that Odds and Trust do not carry over this good performance to all datasets and attacks. Also, both variants of ReBeL perform well in the low perturbation norm regime.

E.4 Comparison of Running Time

Table 7 reports the wall-clock running time (in minutes) of the different detection methods per-fold, averaged across all attack methods. Trust consistently has the least running time, while both variants

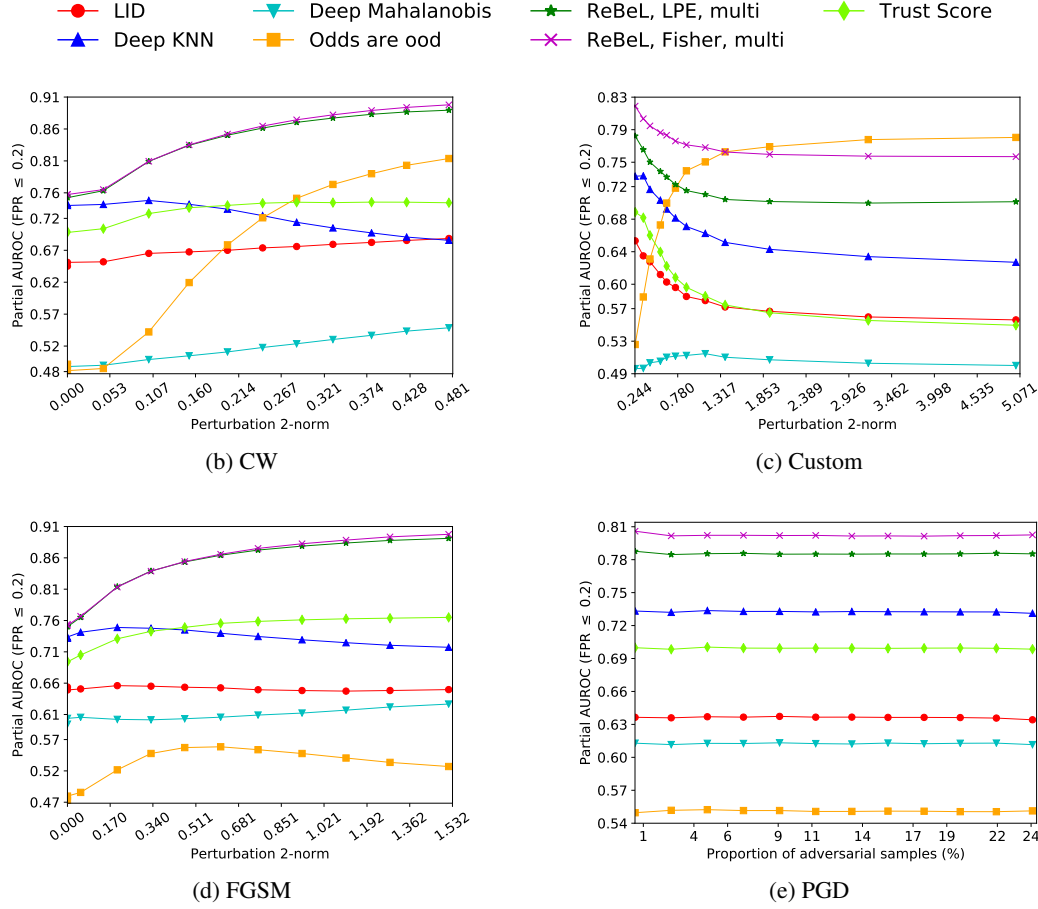


Figure 7: SVHN experiments: pAUC-0.2 for different attacks.

of ReBeL have low running time as well. The running time of Mahalanobis is comparable to ReBeL on MNIST and SVHN, but is higher on CIFAR-10. This is because Mahalanobis performs a search for the best noise parameter at each layer using 5-fold cross-validation, which takes a longer time on the Resnet-34 DNN for CIFAR-10. Odds and LID have much higher running time compared to the other methods. For each test sample, Odds computes an expectation over noisy inputs (from a few different noise parameters), which increases its running time as the size of the DNN increases. The computation involved in estimating the LID features at the DNN layers increases with the sample size used for estimation and the number of layers.

| Dataset | ReBeL, Fisher | ReBeL, LPE | Mahalanobis | Odds | LID | DKNN | Trust |
|----------|---------------|------------|-------------|--------|--------|-------|--------|
| CIFAR-10 | 2.73 | 2.18 | 15.08 | 142.94 | 49.74 | 11.99 | 0.5292 |
| SVHN | 6.37 | 5.01 | 4.19 | 33.60 | 100.80 | 23.54 | 0.60 |
| MNIST | 0.92 | 0.85 | 1.18 | 6.79 | 6.96 | 1.73 | 0.24 |

Table 7: Average wall-clock running time per-fold (in minutes) for the different detection methods.

The computational cost of ReBeL at prediction (test) time can be roughly expressed as $\mathcal{O}(L(d_{\max} N^{\rho} + m^2 + B N))$ when layer pairs are not used, and $\mathcal{O}(L^2(d_{\max} N^{\rho} + m^2 + B N))$ when layer pairs are used. Here d_{\max} is the maximum dimension of the projected layer representations, m is the number of classes, N is the number of samples, B is the number of bootstrap replications used for estimating p-values, and $\rho \in (0, 1)$ is an unknown factor associated with the approximate nearest neighbor queries (that are sub-linear in N). We note that the p-value calculation can be made faster and independent of N by pre-computing the empirical (class-conditional) CDF of

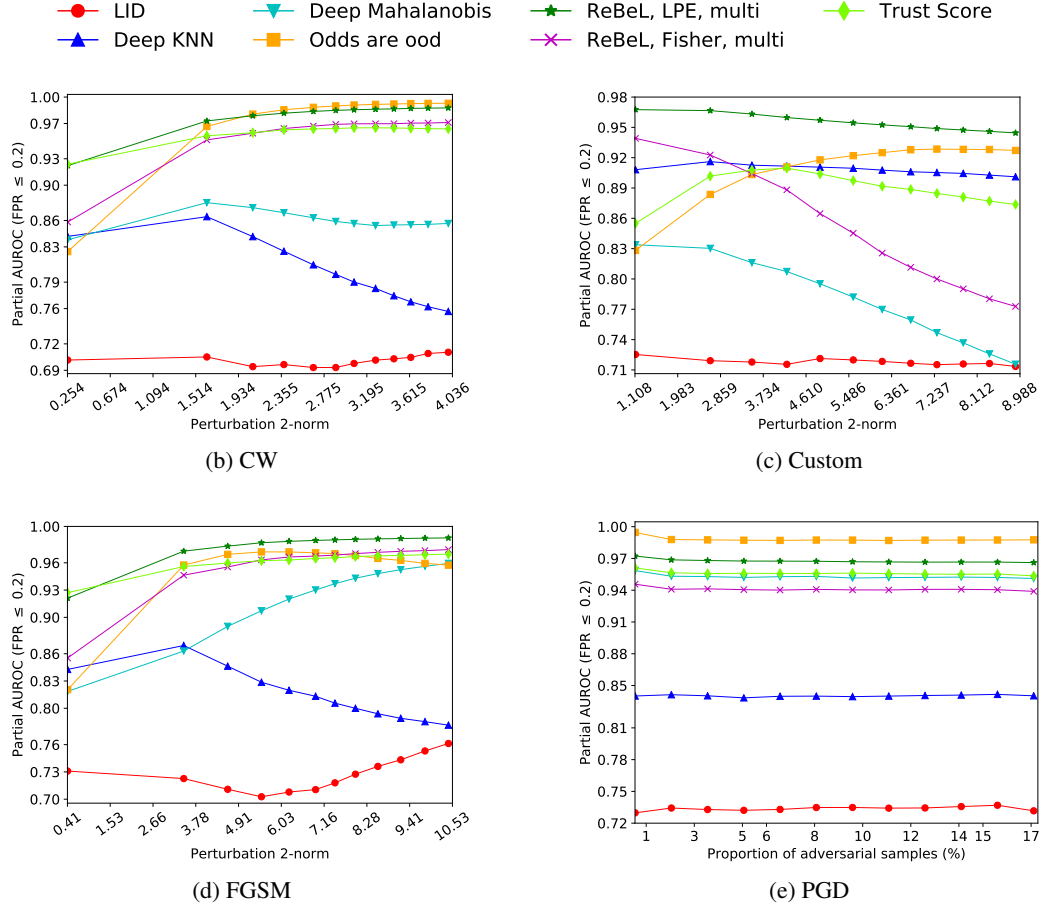


Figure 8: MNIST experiments: pAUC-0.2 for different attacks.

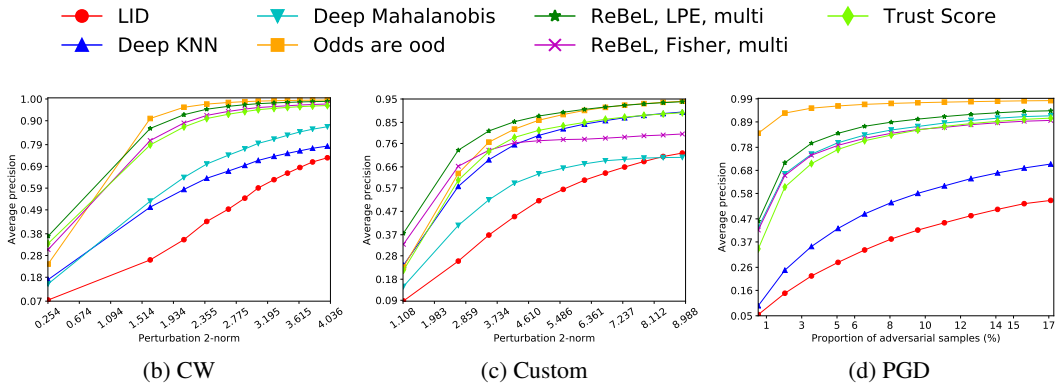


Figure 9: MNIST experiments: average precision for different attacks.

the test statistics per layer. For DNNs with a large number of layers, we recommend not calculating p-values from the layer pairs.

E.5 Performance of ReBeL with Different Test Statistics

The performance of ReBeL (using Fisher’s method) with the four test statistics proposed in § 3.7 and Appendix B is compared on the CIFAR-10, SVHN, and MNIST datasets in Figures 10 through 12. The plots show average precision as a function of the perturbation norm for the CW, Custom, and

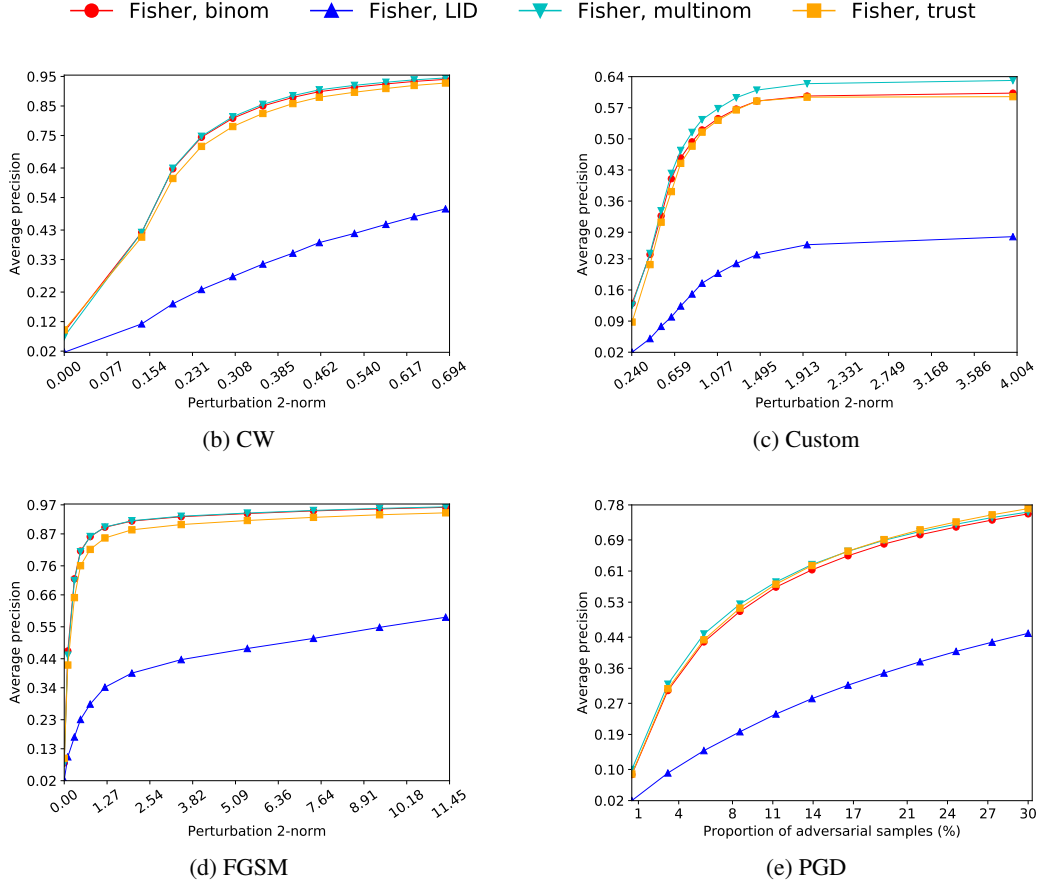


Figure 10: Average precision of ReBeL with different test statistics on CIFAR-10.

FGSM attacks, and average precision as a function of the proportion of adversarial samples for the PGD attack. Notably, the test statistic based on LID performs poorly in all cases. On CIFAR-10 and SVHN, the binomial and trust score based test statistics have comparable performance to the multinomial test statistic on all except the custom attack, on which the multinomial based test statistic performs better. We observe a different trend on the MNIST dataset, where the trust score and binomial based test statistics perform better than the multinomial test statistic, notably on the custom attack.

E.6 Performance Improvement From Class Conditioning

Here we empirically show that calculating class-conditional (instead of marginal) attributes at the DNN layers can lead to performance improvement for an existing adversarial detection method LID [23]. In the work of Ma *et al.* [23], the LID estimates of the DNN layer representations are based on mini-batches of samples drawn from the marginal data distribution. Instead, we propose to use the DNN predicted class of a test sample, and estimate LID at the layers relative to samples drawn from the predicted class (*i.e.*, the class-conditional distribution). Figure 13 plots the average precision and pAUC-0.2 metrics comparing the performance of LID with its class-conditional extension on four attack methods applied on the CIFAR-10 dataset. It is clear that the class-conditional extension has a notable improvement in performance on all except the PGD attack (where the performance is comparable).

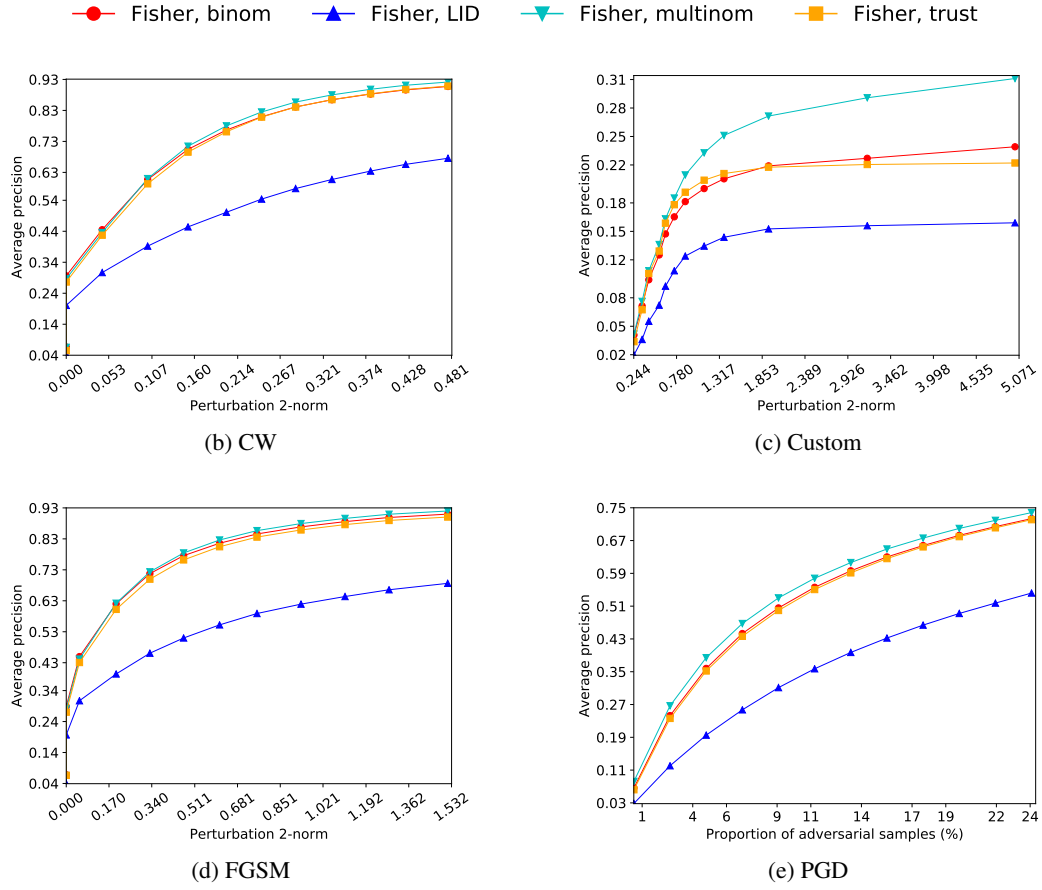


Figure 11: Average precision of ReBeL with different test statistics on SVHN.

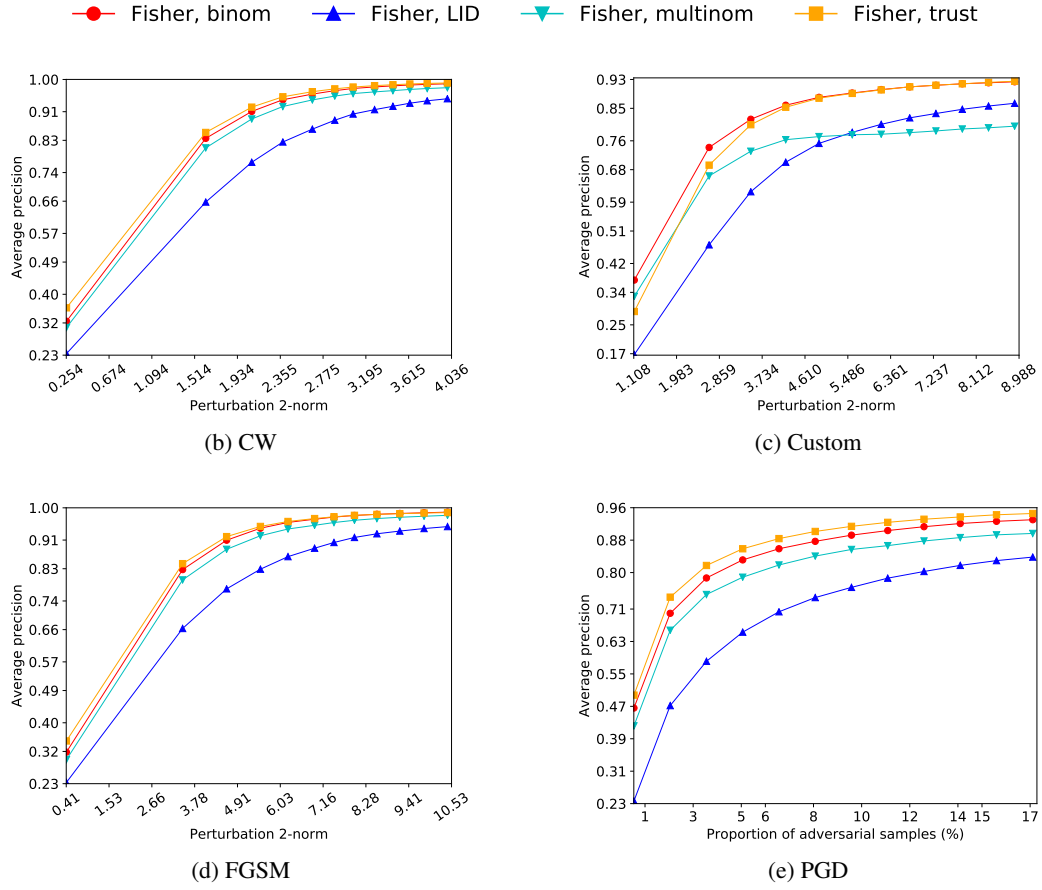
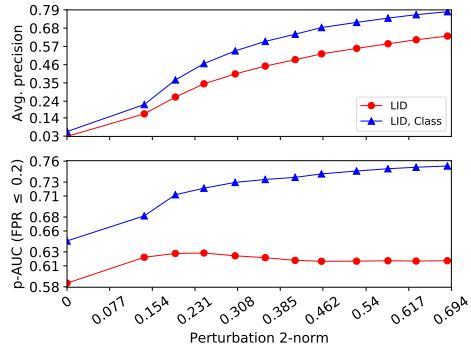
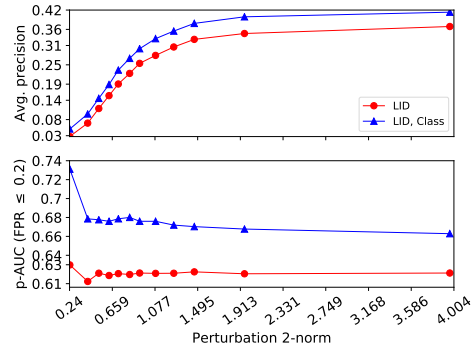


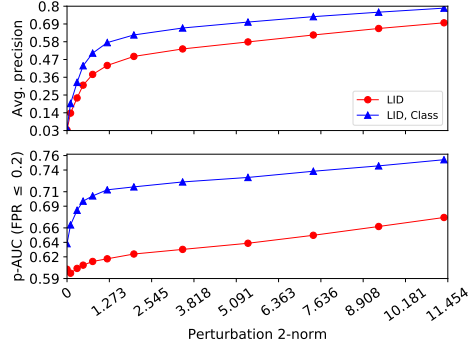
Figure 12: Average precision of ReBeL with different test statistics on MNIST.



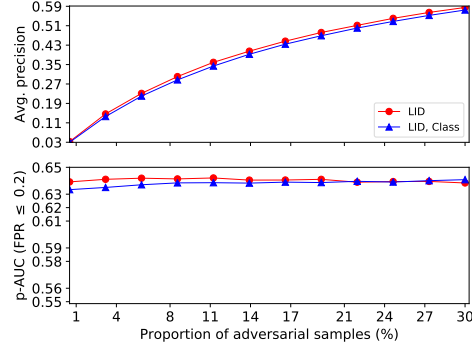
(a) CW



(b) Custom



(c) FGSM



(d) PGD

Figure 13: Average precision and pAUC-0.2 of the class-conditional extension of LID for different attacks on CIFAR-10.